

Chapter 4

Density functional theory as a screening method for dense metal membranes

4.1 Abstract

In this chapter 18 different palladium based membrane materials were simulated in order to determine their suitability as a material for hydrogen impurity enrichment. The alloys were represented using $2 \times 2 \times 5$ atomic slab models comprised of palladium, with varying compositions of different metals including common palladium additives (Au, Ag, Cu), and metals known for their resistance against aggressive environments (Zr, Cu). From the alloy compositions tested 16/18 were stable, with Cr containing alloys unable to form a stable system. The 16 remaining alloys were then tested with hydrogen, and each of the ISO 14687-2 impurities adsorbed on the 4 available surface sites for hydrogen adsorption. The results were that the impurities could be split into four broad groups. Inert impurities included NH₃, CO₂, N₂, He, Ar and formic acid, which did not interact with the surface of the alloys. Oxidising impurities included H₂O and O₂, which pure palladium alone was completely resistant against. The effect could be amplified through the addition of Au and Ag, with PdAu₂₀ being the best performing alloy for resisting these impurities. Carbonaceous impurities included CO and CH₄ where PdAu₂₀ was again the best performing alloy, with an average binding energy of CO and CH₄ of around $\times 0.4$ and $\times 0.5$ compared to binding of H. Finally sulphurous atmospheres were tested using H₂S where PdCuZr and PdAuZr alloys were the best performing. These alloys showed an average binding energy of $\times 0.52$ and $\times 0.49$ compared to H. Formaldehyde was a special case where no alloy composition was found to resist binding.

This study shows that DFT can be used to give an indication on the suitability of a palladium alloy membrane for its desired purpose. It also shows that while the effects of some impurities on the surface of a palladium alloy membrane can be completely mitigated, many cannot be inhibited completely. A number of alloys were identified as

the best options for hydrogen impurity detection and will be studied experimentally in the following chapters.

4.2 Introduction

Metal membranes operate by selectively dissociating hydrogen, which then allows the hydrogen atoms to subsequently permeate through the bulk of the separation layer. The problem in using palladium membranes as a material for performing hydrogen impurity enrichment is that many hydrogen impurities are also capable of adsorbing onto, and interacting with palladium membranes. The impact of this adsorption can vary depending on the molecule, Carbon monoxide for example will simply adsorb onto the surface and result in competitive adsorption between the hydrogen and impurity. Sulphur containing impurities present more of a problem since they can potentially react with many metals used for hydrogen separation membranes. The impact of these contaminants can be minimized by designing alloy compositions that have a weaker attraction to the membrane, and therefore will have less of an affect at higher temperatures where these membranes operate.

Physically testing each potential membrane composition would be time consuming and costly due to the high price of palladium, the time required to synthesise specific membrane compositions, and performing the tests. Simulations provide a solution to this, allowing potential alloys to be quickly screened for their interaction strength with each individual ISO 14687-2 impurity, avoiding the costly and time consuming process of manufacturing each alloy composition.

In this chapter, 18 dense metal alloy membranes will be simulated using DFT density functional theory as described in section 3.1 [1, 2, 3]. The metals will first be evaluated in terms of their ability to form a stable alloy, with low risk of segregation, or failure. All stable metals will then be simulated with either hydrogen, or an ISO 14687-2 impurity on the surface, and its binding energy calculated. The results will be evaluated using the ratio of binding energy of adsorbent to binding energy of hydrogen (σ) on the same metal as shown in equation 4.1 where E_{ads} is the binding energy, i is the simulated impurity on the surface of the metal alloy, and H is hydrogen.

$$\sigma = E_{i_{ads}} / E_{H_{ads}} \quad (4.1)$$

The metallic compositions with the lowest value for σ represent the best simulated material for dealing with that impurity. A high value of σ indicates that the metal is more reactive with the impurity molecule, whereas a σ value of 1 or lower indicates that the ability for the impurity to adsorb on the surface is equal to, or lower than that of hydrogen, and therefore has a weaker interaction.

4.3 Results and discussion

4.3.1 Stability of palladium alloy compositions and ISO 14687-2 impurities

In order to perform the simulations, first an appropriate slab model of each alloy must be created. The structure of these slabs is shown in section 3.1.2. The metals chosen to substitute into the palladium lattice were common palladium alloys (Au, Cu, and Ag) and metals which have previously shown a resistance to sulphur. Zr[4] and Cr[5] are commonly used additives in steel to improve it's corrosion resistance in acidic environments and were decided to be ideal candidates. Once simulated the total energy of the system was compared to the sum of the energy levels of the component atoms. The results of this analysis are shown in table 4.1. All alloys were stable except for the Cr containing alloys which could not converge to a suitable solution.

Similarly each ISO 14687-2 impurity was simulated and the results of these can be found in table 4.2. The parameters used to simulate these molecules can be found in the appendix.

Table 4.1: Simulated total energy values of alloy slabs

Alloy/Metal Composition	Total Energy (ry)
Pd	-6653.38
PdAg ₂₃	-6774.37
PdAu ₁₀	-7545.53
PdAu ₂₀	-8437.613
Pd ₆₀ Cu ₄₀	-5703.15
Pd ₈₀ Cu ₂₀	-6178.29
Pd ₇₀ Au ₂₀ Zr ₁₀	-8389.61
Pd ₇₀ Cu ₂₀ Zr ₁₀	-6130.29
Pd ₇₀ Ag ₁₀ Zr ₂₀	-6605.75
PdZr ₁₀	-6605.45
PdZr ₂₀	-6557.46
Pd ₇₀ Au ₂₀ Ag ₁₀	-8485.99
Pd ₇₀ Au ₂₀ Cu ₁₀	-8200.05
Pd ₇₀ Cu ₂₀ Ag ₁₀	-6226.71
PdCr ₁₀	-
PdCr ₂₀	-

Table 4.2: Simulated total energy values of ISO 14687-2 impurities

Gas	Total Energy (kJ × 10 ⁻²¹)
H	-2.01
N ₂	-123.91
O ₂	-180.86
CO	-130.93
CO ₂	-221.95
NH ₃	-1933.22
Ar	-208.10
CH ₄	-50.73
Formaldehyde	-136.13
Formic Acid	-227.08
H ₂ S	-150.36
He	-12.62
H ₂ O	-95.99

4.3.2 Hydrogen and Impurity adsorption on palladium alloy membranes

Hydrogen

The hydrogen binding energy on the surface of palladium is a key value for the purpose of this study. The affinity for a palladium alloy to adsorb on the surface is the initial step for hydrogen permeation, and below a certain thickness becomes the rate limiting step. As expected all alloys had an affinity for hydrogen binding and these values matched what is generally found in literature. These values will be compared to the binding energies of other impurities on the alloys in order to determine their resistance to the impurity. The binding energies of hydrogen on a the Pd slab system is shown in figure 4.1. In a Pd system hydrogen preferentially adsorbs on the FCC and top sites at relativley even energies. At both of these sites hydrogen is able to form a stable system without being affected by other forces. HCP and TOP sites have a lower preference for hydrogen binding and this is likely due to the influence of competition by neighbouring sites which can provide higher stability. The average binding energies of hydrogen on the surface of all palladium alloy slab systems are shown in figure 4.2.

All alloys show a decreased preference towards hydrogen binding compared to pure palladium. This is due to hydrogen adsorption energies being closely related to the catalytic activity for hydrogen dissociation of the individual metal elements. The effect appears to be less prevalent for binary alloys with elements with a larger atomic size such as silver which is likely due to the larger atomic size creating a larger area for hydrogen to adsorb within fcc site of the crystalline lattice, which is one of the preferential sites for H adsorption. Zr and Au do not follow this trend however which indicates that the

Hydrogen adsorption sites on Pd

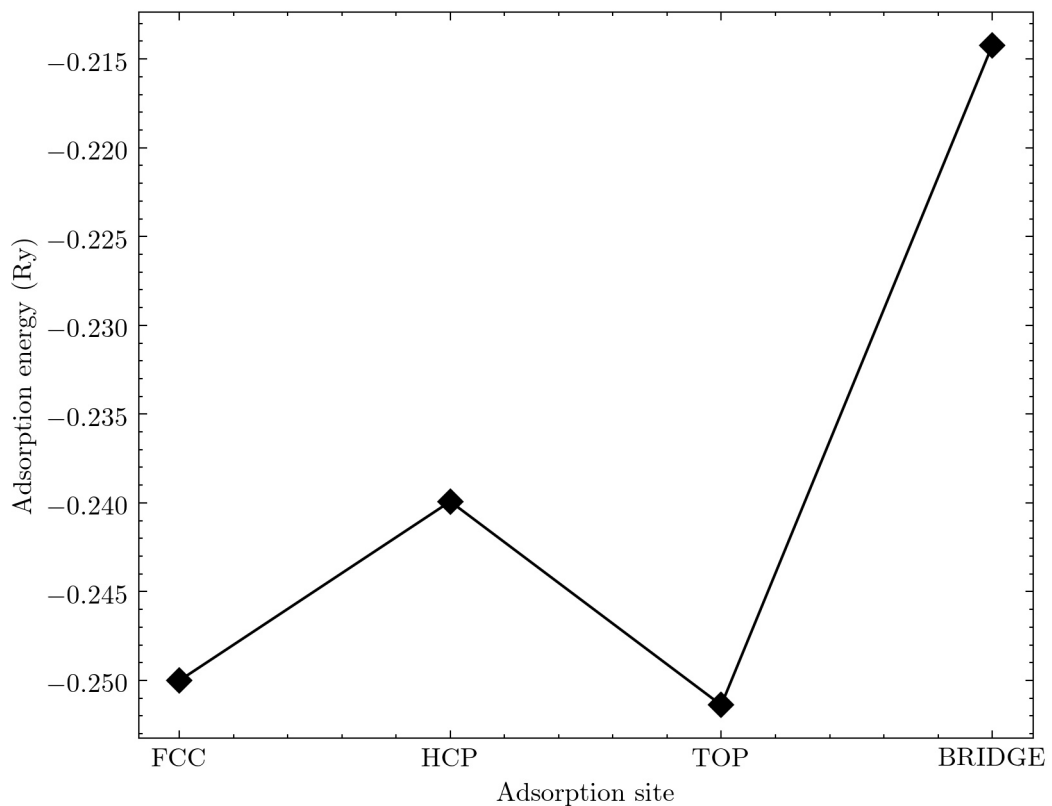


Figure 4.1: Adsorption energy of H for each site on a 2x2x5 Pd slab

Table 4.3: Correlation coefficient of Ag, Au, Cu, Zr addition to Pd with binding energy of H

Metal	Correlation coefficient
Ag	-0.024666
Au	0.259205
Cu	0.019221
Zr	0.347930

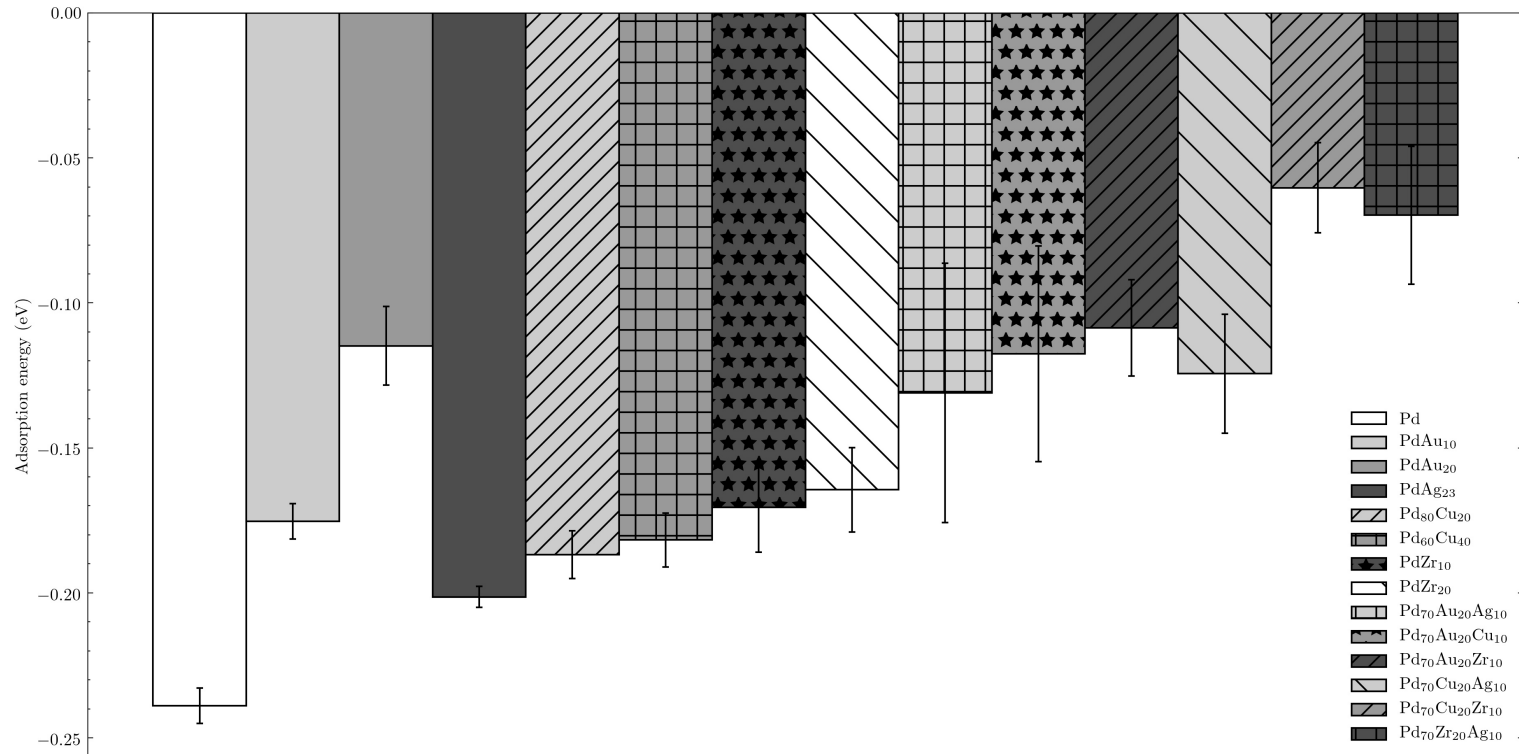
catalytic activity is affected more by electronic interactions than surface geometry. In all cases reduction in palladium from the surface results in lower catalytic activity for hydrogen adsorption which is also likely to be due to the average reduction in number of top sites available for adsorption, which other than FCC is one of the preferential adsorption sites.

The ternary alloys with the highest catalytic activity were PdAuAg and PdCuAg which previous experimental results showing that these alloys have higher permeability than other ternary alloys. All Zr containing alloys had lower catalytic activity showing that for hydrogen permeation Zr has the greatest inhibiting effect. The detrimental effects of Zr to the catalytic activity can be lowered by the addition of Au, Ag, or Cu however all are still lower than binary alloys.

The correlation coefficient for the presence of each metal and it's effect on the resulting adsorption energy was calculated and is shown in table 4.3. It shows that the resulting inhibiting effect of each element follows the order Ag<Cu<Au<Zr.

This binding energy of hydrogen is an important benchmark for the following tests and will be compared to the resulting binding energies for other impurities. If these impurities show a lower binding energy value when compared to hydrogen then they will be preferntially adsorbed and less suitable for use for that type of impurity. It also reveals that the composition of the membrane can largely effect the catalytic activity for dissociation of hydrogen in itself. As membranes become thinner this will result in a shift of the limiting step to catalytic activity and therefore this value must also be optimised to ensure the highest flux can be achieved, however such work is outside the scope of this study.

Hydrogen adsorption

Figure 4.2: Average binding energy of H_2 on the surface of palladium and palladium alloy slabs

Helium, Nitrogen, Carbon Dioxide and Argon

Helium, Nitrogen, Argon, and CO₂ all represent the inert components in fuel cell hydrogen which do not interact with the electrocatalyst and are therefore also likely to be inert to palladium membranes. The binding energies of these molecules on the surface of all the simulated palladium alloy slab systems are shown in figures 4.3 (He), 4.4 (N₂), 4.5 (CO₂) and 4.6 (Ar). All these systems showed a positive binding energy meaning that no competitive adsorption will take place between these gases and hydrogen for the surface adsorption sites.

Carbon Monoxide

CO adsorption was performed by adsorbing the gaseous molecule by the C atom as is normal for CO binding on metallic surfaces [6]. All systems showed binding preference towards CO. The results of the simulations and their binding energies compared to that of hydrogen on the same alloy are shown in figure 4.8. No alloys showed an aversion to CO binding therefore all of the simulated alloys, regardless of their preference to H₂, will likely experience some competitive adsorption and therefore inhibition when CO is present.

The pure Pd system showed a clear preference to CO binding over hydrogen, this matches previous experiments performed to investigate this. [7] Figure 4.7 shows the binding energy on each site compared to that of H calculated in section 4.3.2. The fcc system shows a clear preference for CO on the FCC, HCP and TOP sites, while still preferring to bind to H on the BRIDGE site. This is most prevalent for the FCC site which has a lower binding energy of around -0.55 eV, with HCP and TOP sites showing a drop in around -0.35 and -0.3 eV respectively. However since the top site still shows a preference for H binding which represents around 41% of the binding sites. While this may indicate that these sites are still available for hydrogen permeation, when bulk diffusion is modelled using kinetic monte carlo simulations that hydrogen travels through the bulk by relaxing the lattice around the fcc and hcp sites to facilitate transport. [8] Therefore the blocking of these sites is likely to have a severe effect on hydrogen permeation.

Of the systems tested PdAu₂₀, PdAg₂₃, and Pd₇₀Au₂₀Cu₁₀ all showed marginal preference for hydrogen binding over CO binding. Binding of CO on Au and Ag surfaces has previously been studied and concluded that these metals do not interact with CO under normal circumstances, and will only adsorb through way of material defect or alloying. [9] [10]

By far the worst performing metal for inhibiting the effect of CO were all Zr containing alloys, and Pd₆₀Cu₄₀. Zr readily forms a bond with C, and even has its own unique branch of chemistry referring to such compounds.[11] Zirconium is also a common complex used in homogeneous refractory catalysts for reforming hydrocarbon compounds.[12] Therefore the evidence suggests that Zr naturally has a high affinity towards forming carbon bonds and is not a suitable additive for CO resistant membranes.

Similarly Cu has been previously studied and found to readily adsorb CO on its

He adsorption

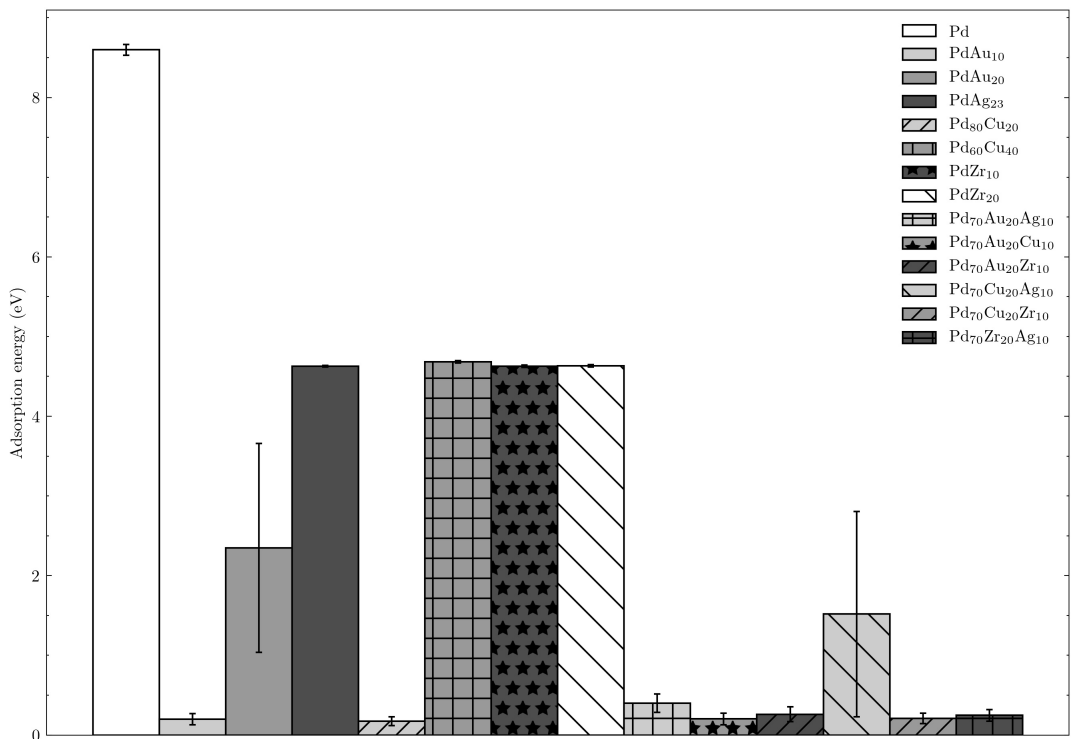


Figure 4.3: Average binding energy of He on the surface of palladium and palladium alloy slabs

N_2 adsorption

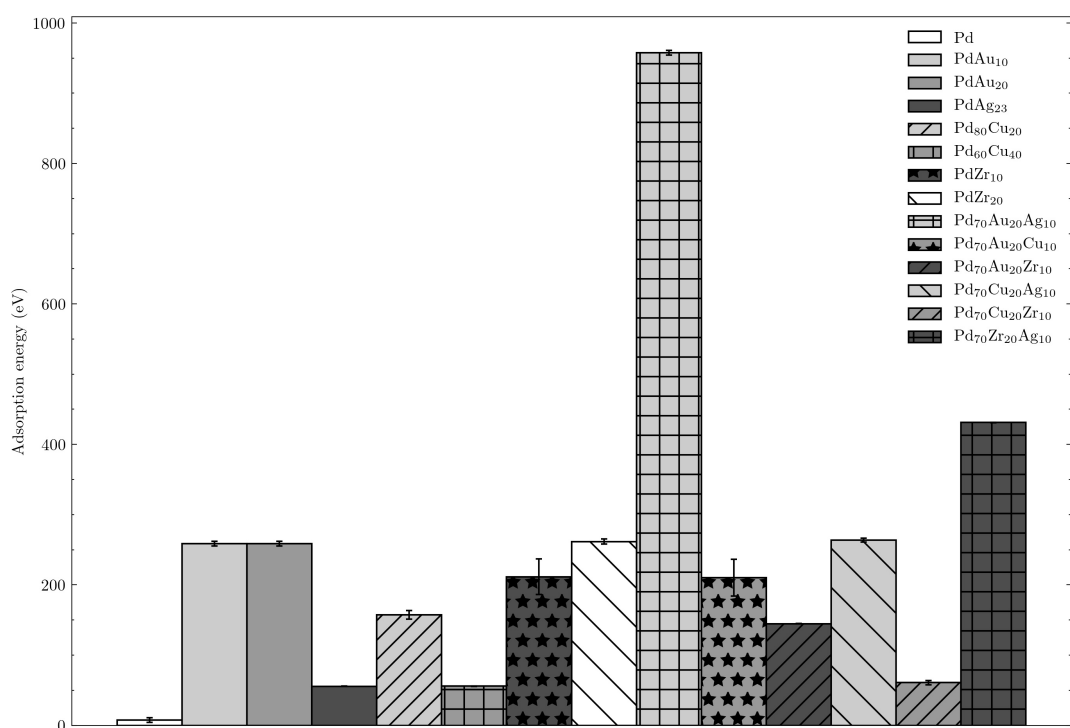


Figure 4.4: Average binding energy of N_2 on the surface of palladium and palladium alloy slabs

CO₂ adsorption

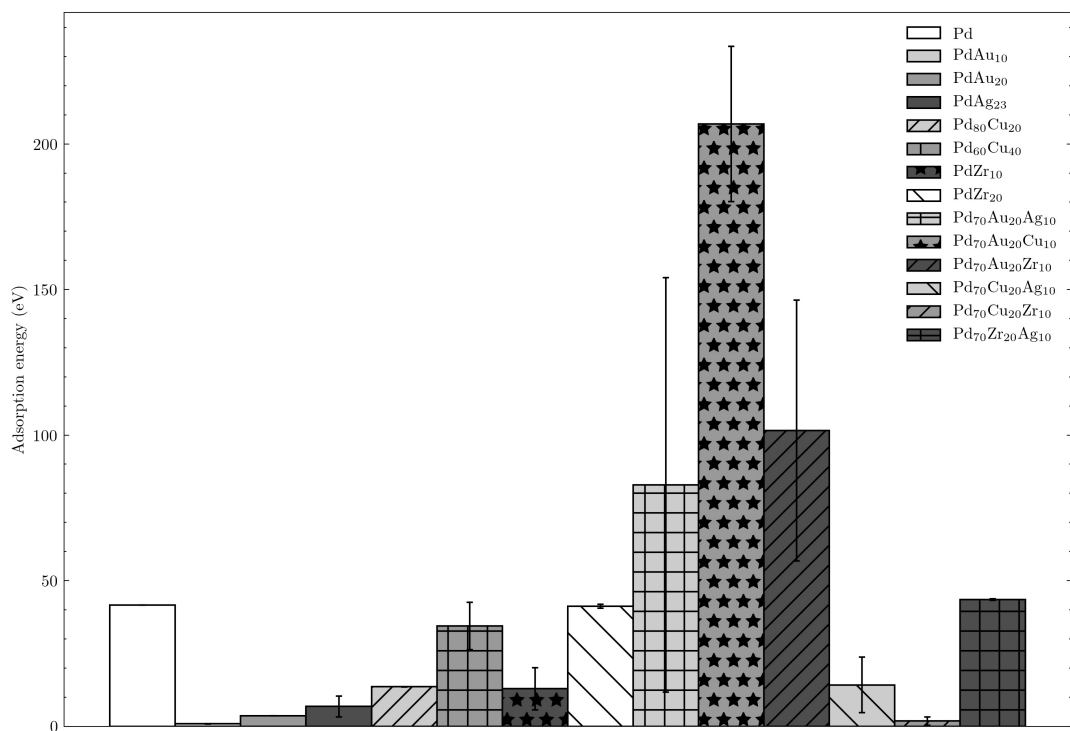


Figure 4.5: Average binding energy of CO₂ on the surface of palladium and palladium alloy slabs

Ar adsorption

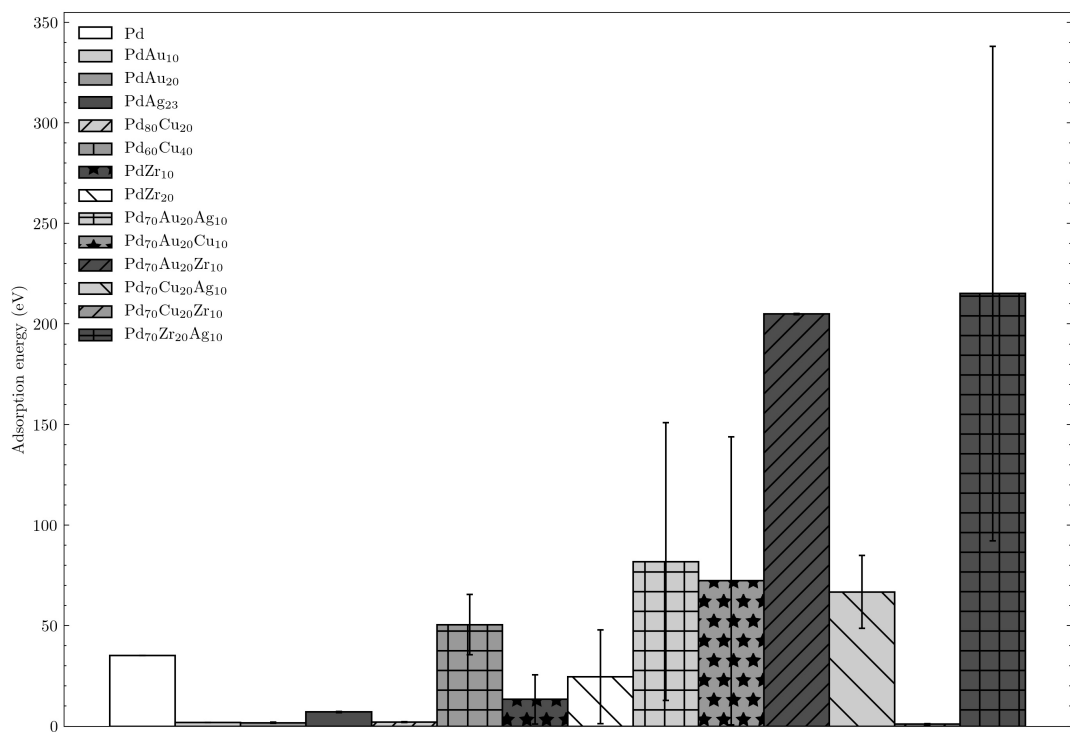


Figure 4.6: Average binding energy of Ar on the surface of palladium and palladium alloy slabs

CO adsorption sites on Pd compared to H

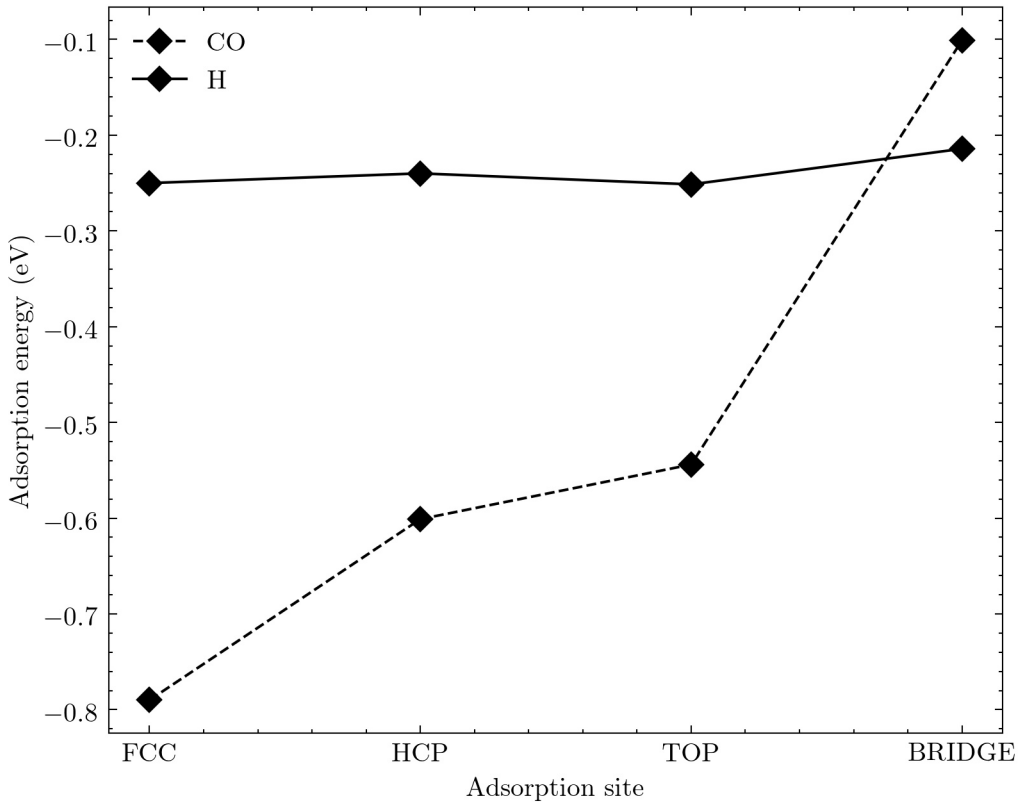


Figure 4.7: binding energy of H and CO for each site on a 2x2x5 Pd slab

surface. [9] This does not appear to be an issue for PdCu_{20} alloys indicating that this level of Cu is too low to have such an effect. The $\text{Pd}_{60}\text{Cu}_{40}$ alloy on the other hand has a much higher binding preference for CO than its sister hydrogen system. $\text{Pd}_{60}\text{Cu}_{40}$ is different from other systems in that the crystalline structure transitions to a BCC lattice. [13] BCC structures only have two different sites available for hydrogen binding, BRIDGE and HCP. [14] This change in structure combined with the Cu's availability to bind with C likely accounts for the large discrepancy.

CO adsorption

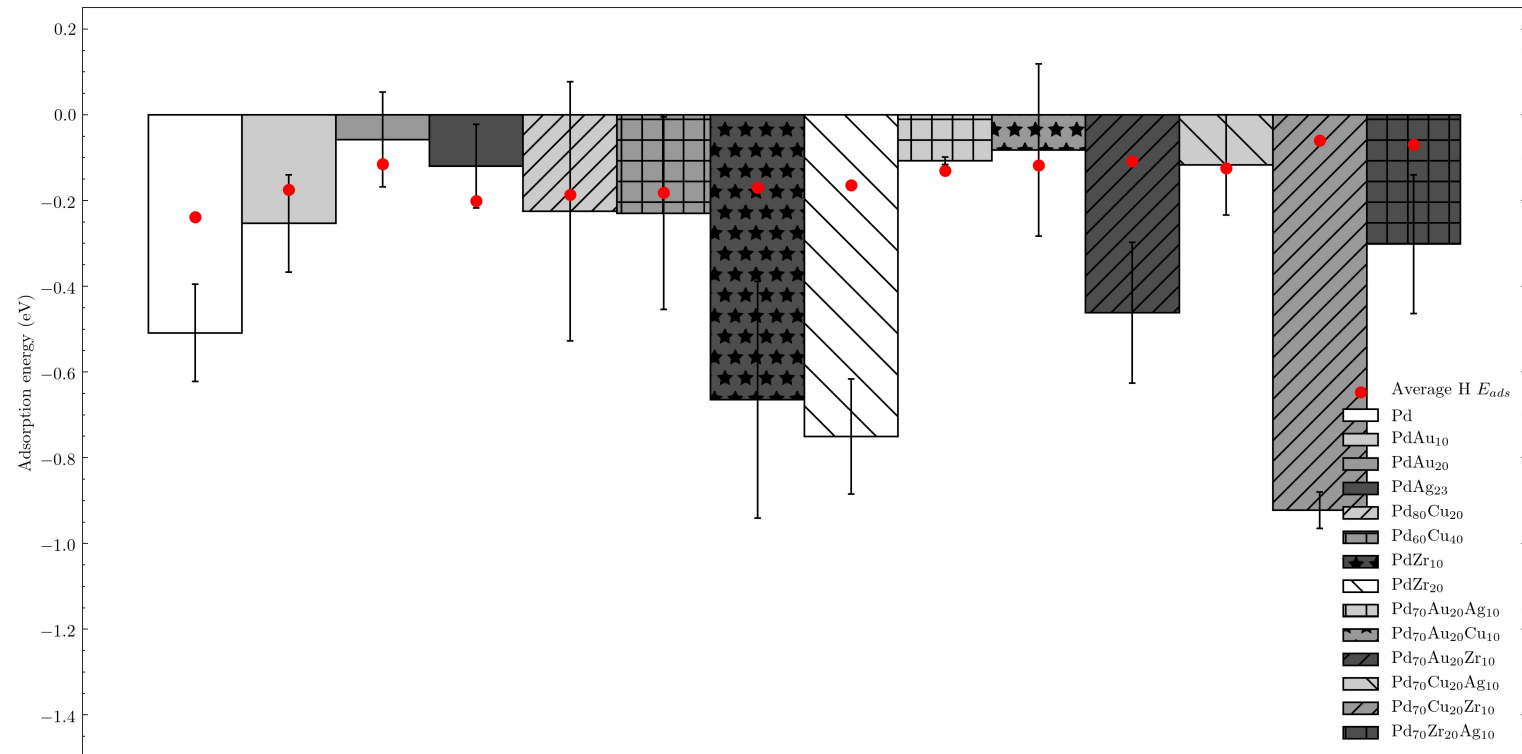


Figure 4.8: Average binding energy of CO on the surface of palladium and palladium alloy slabs

NH₃ adsorption

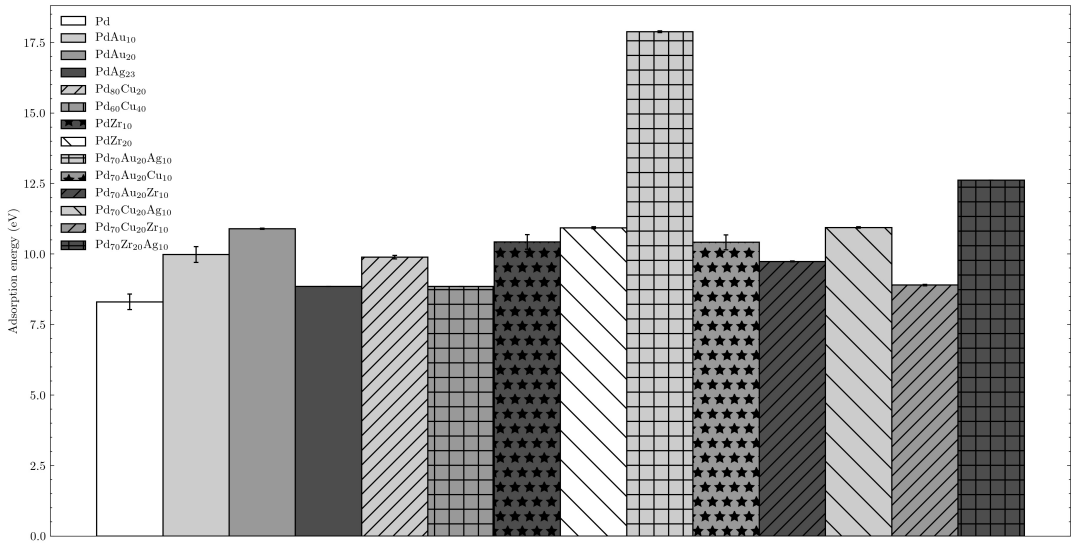


Figure 4.9: Average binding energy of NH₃ on the surface of palladium and palladium alloy slabs

Ammonia

The results of the ammonia simulations are shown in figure 4.9. Of the tested material compositions, neither palladium or any alloy showed an ability to readily bind with Ammonia, this was also true across all sites on the fcc and bcc lattice. This is consistent with the experimental results of Lundin et al [15] and the previous simulations by Herron et al [16]. It should be noted that the paper by Herron [16] found that while ammonia itself did not bind with the surface of palladium, radicals which can be created from ammonia such as imidogen (NH) and azanide (NH₂) will readily form bonds. It is however extremely unlikely that these compounds wil be present in fuel cell hydrogen, and in the unlikely event they are they will likely instantly reform into the more stable NH₃. It can be concluded therfore that NH₃ will create no challenges for the operation of palladium membranes.

Oxygen and Water

Since O₂ is a symetrical molecule binding was performed similarly to H₂ in section 4.3.2, the results of which are shown in figure 4.10. Alloys consisting mainly of noble metals (Pd, Ag, Au) typically did not readily bind with oxygen. Whereas alloys containing non-noble metals (Zr and Cu) showed a preference towards oxygen binding. This can pose an issue during enrichment and will likely lead to either the formation of oxides on the surface of the membrane, or catalyse a reaction between either oxygen and hydrogen, or oxygen and one of the other gaseous impurities. In the former the formation of oxides creates a shift in the lattice parameter, similar to the $\alpha - \beta$ transition seen in pure

palladium membranes (figure 2.6)[17] and cause membrane failure. In the latter results from hydrogen impurity can be thrown off. Therefore if oxygen is expected in the sample Zr and Cu containing alloys should be avoided.

Water adsorption was performed by attaching the O atom to each available site as per previous studies. [18] The results are shown in figure 4.11 and follow the same trend as the O₂ results discussed above. One important caveat when considering water binding on the surface of metals is the ability for H₂O molecule to form hydrogen bonds with neighbouring molecules.[19] While this study only considered the influence of a single water molecule, in real tests the system will likely have a number of water molecules present. The effect of the hydrogen bond would likely result in the further stabilisation of future water molecules onto the surface, creating an exponential increase in adsorbed H₂O. [19] Care should also be taken, as previous studies on other metallic systems have shown that the binding of water often leads to subsequent dissociation, and formation of a metal oxide and hydrogen. Leading to the same problems with oxidation as previously discussed. [20]

In conclusion noble metals appear to be the best alloying compounds to protect against the influence of H₂O and O₂. This is to be expected as these metals are traditionally resistant to oxidation. It should be noted however that while this study focused on binding of water on the membrane, it does not take into account adsorption on any other components and fittings on a system. Water in particular is notoriously difficult to remove from a system due to its availability for binding on metal surfaces.[21] Therefore while reducing its effect on the membrane solves one problem, its effect on the overall system still has to be considered.

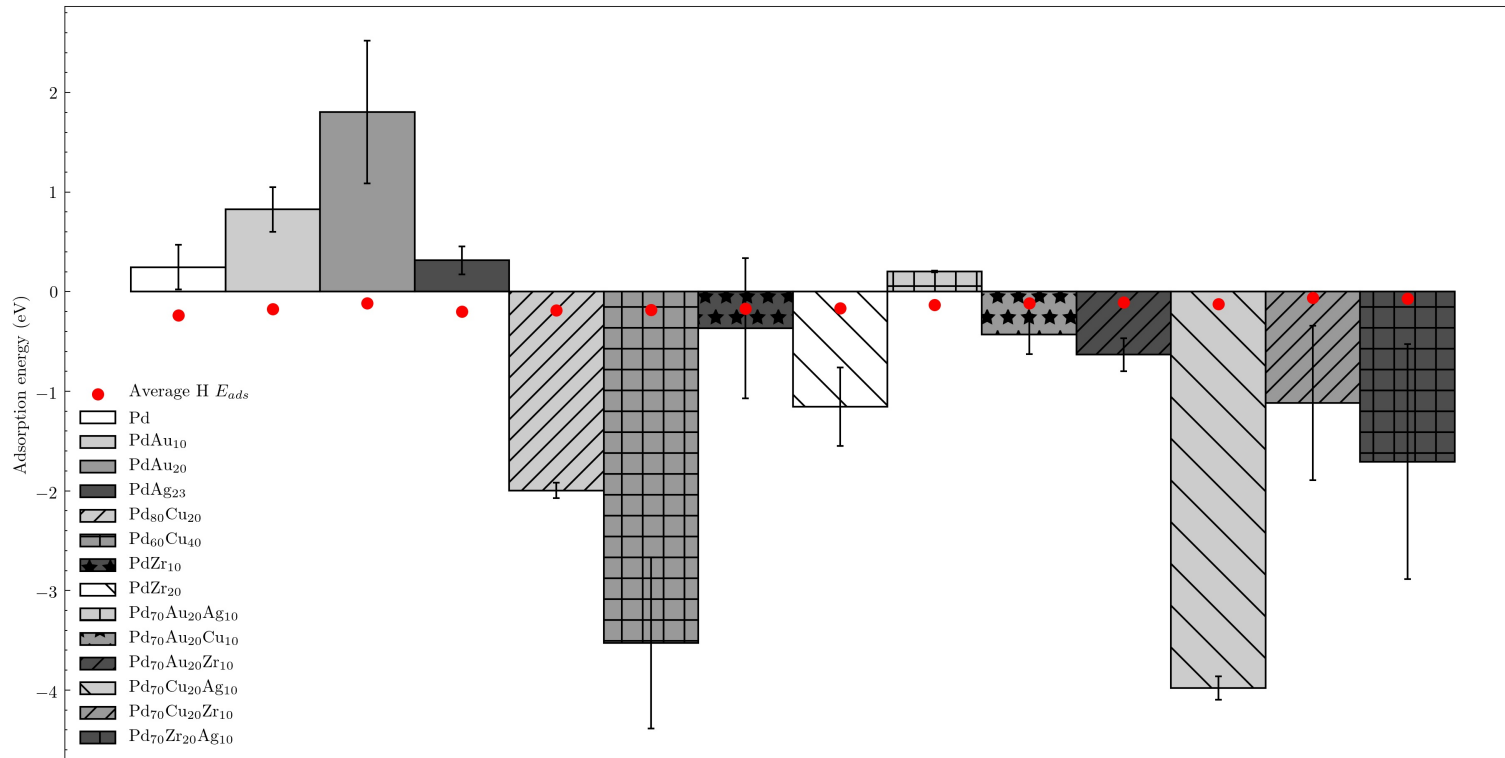
O_2 adsorption

Figure 4.10: Average binding energy of O₂ on the surface of palladium and palladium alloy slabs

H₂O adsorption

122

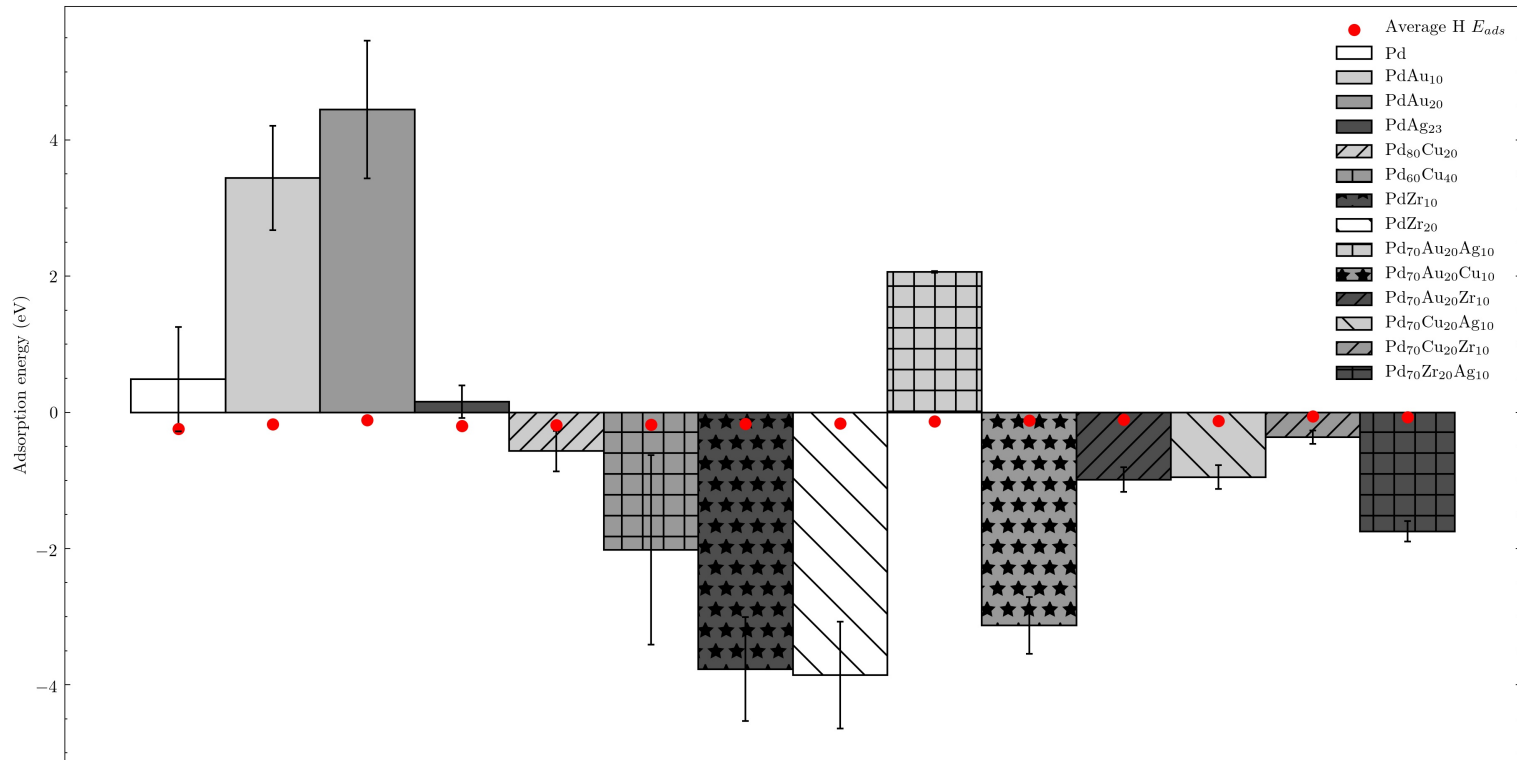


Figure 4.11: Average binding energy of H₂O on the surface of palladium and palladium alloy slabs

Methane

Methane was adsorbed onto the surface of the Pd slab systems using one of the hydrogen molecules as has previously been performed in literature. [22] The results of the simulations are shown in figure 4.13.

All simulated metals seem to have the ability to bind CH_4 to its surface. Intuitively this seems reasonable since the atom binding to the surface is H_2 , which we have already proven has the ability to bind to all Pd alloy models. The molecule also features a carbon molecule which from our CO simulations in figure 4.8 will also preferentially bind to the surface of the Pd slab models, at a higher preference than hydrogen. The results of the CH_4 simulations seem to follow the general trend of it's sister CO results, however at a weaker level. All simulations were unstable which is shown by the large error values showing large swings in the results from each simulation. Therefore it is likely that in many simulations, while CH_4 is stable on the surface, could not find the most stable coordination due to competing forces acting from the hydrogen atoms, and the carbon atom.

The binding energies of CH_4 on each site in the Pd system are shown in figure 4.12. Similarly to CO, the CH_4 molecule has a higher preference to the FCC and HCP sites than H. Unlike CO, CH_4 does not bind as strongly to the TOP site as CO. The reason for the strong binding preference to the FCC and HCP sites is likely due to the fact that while the H atom is bound within the HCP and FCC sites, the C atom and other H atoms will bind to the surrounding metallic atoms in the crystalline lattice, stabilising the molecule in those sites. On the TOP and BRIDGE sites this does not happen, and since the H atom is bound more strongly to C through a covalent bond, the resulting energy available for binding on these sites is lower than it would be if the molecule was pure hydrogen.

In terms of resistance to CH_4 binding, the conclusions reached in the section discussing the results of CO still hold true. All alloy compositions with high percentages of Au and Ag showed higher resistance to CH_4 binding, whereas Cu and Zr containing molecules performed worse.

Past studies performing CH_4 binding on metallic surfaces found that in some cases the H atom could dissociate from the molecule, creating CH_3 and H. [23] In this particular application such a reaction would result in the liberated H atom permeating through the membrane, leaving CH_3 on the retentate side. While this changes the composition of the retentate gas, from a measurement perspective it should not pose much of an issue. The ISO 14687-2[24] standard specifies a total hydrocarbon level and therefore any CH_3 that is produced should be detected using previously outlined techniques. [25]

What may pose a larger issue is that in the study performed by Herron [16], it was found that similar to Ammonia, CH_4 based radicals will bind more strongly to the surface than CH_4 resulting in an increasing poisoning effect. It is unknown whether the hydrogen dissociation effect previously discussed would continue to occur with these radicals, but in the case it does, the result would eventually be carbon deposition on the surface of the membrane. Eventually deactivating the membrane entirely, and throwing off all results due to removal of carbon from the gas.

CH_4 adsorption sites on Pd compared to H

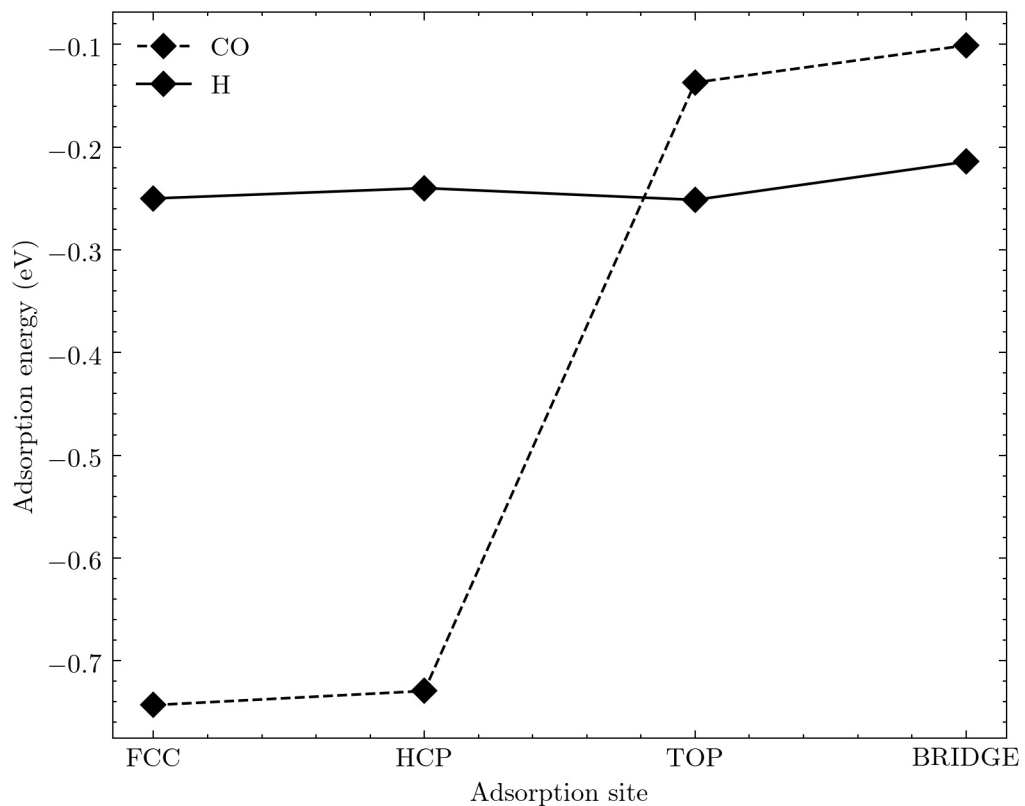


Figure 4.12: binding energy of H and CH_4 for each site on a $2\times 2\times 5$ Pd slab

CH₄ adsorption

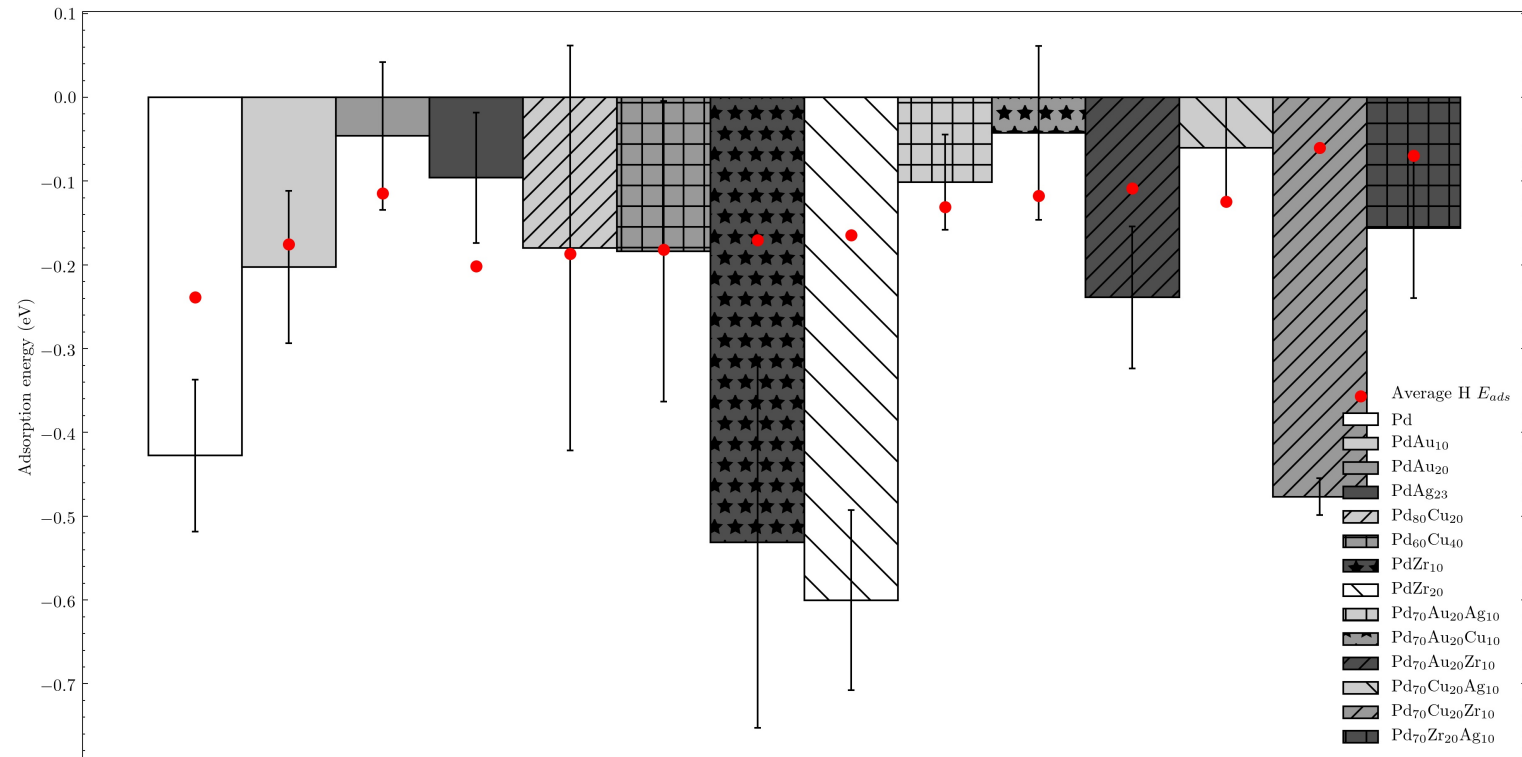


Figure 4.13: Average binding energy of Methane on the surface of palladium and palladium alloy slabs

Formaldehyde and Formic acid

Formaldehyde and Formic acid are similar molecules, with the only difference being one of the hydrogen atoms being replaced with an OH group on formic acid. Both molecules were adsorbed onto the surface using the double bonded O atom perpendicular to the surface of the slab model.[26] The results for the simulations are shown in both figure 4.14 for formaldehyde and figure 4.15 for formic acid.

The results of these simulations vary widely, with formaldehyde showing strong binding ability with Pd and Pd alloy surfaces, while Formic acid appears to reject binding completely. The systems were also largely unstable as indicated by the large error values, which indicates that there are a number of forces acting on each atom on the molecule and therefore multiple stable arrangements other than the one chosen.

This result for formaldehyde is not surprising as formaldehyde is widely known to be effective catalyst for oxidation of formaldehyde, being able to oxidise formaldehyde under the presence of sunlight alone. [27] Therefore it is likely that any mixture containing both formaldehyde and oxygen under the presence of a palladium membrane will likely react, forming carbon dioxide and hydrogen. Additionally palladium alone may be powerful enough to dissociate the formaldehyde molecule, and depending on the coordination of the molecule from H₂ and CO, or hydrocarbon compounds ranging from CH₂ to C₄ and oxygen,[26] the ramifications of which have been discussed previously. Unfortunately out of the tested alloys there does not appear to be a solution to this and further membrane compositions should be screened in order to determine an appropriate material to suppress the effect of formaldehyde.

Past research evaluating Pd surfaces for formic acid oxidation found that Pd surfaces typically reject COH bindings which lines up well with these results. [28]

Formaldehyde adsorption

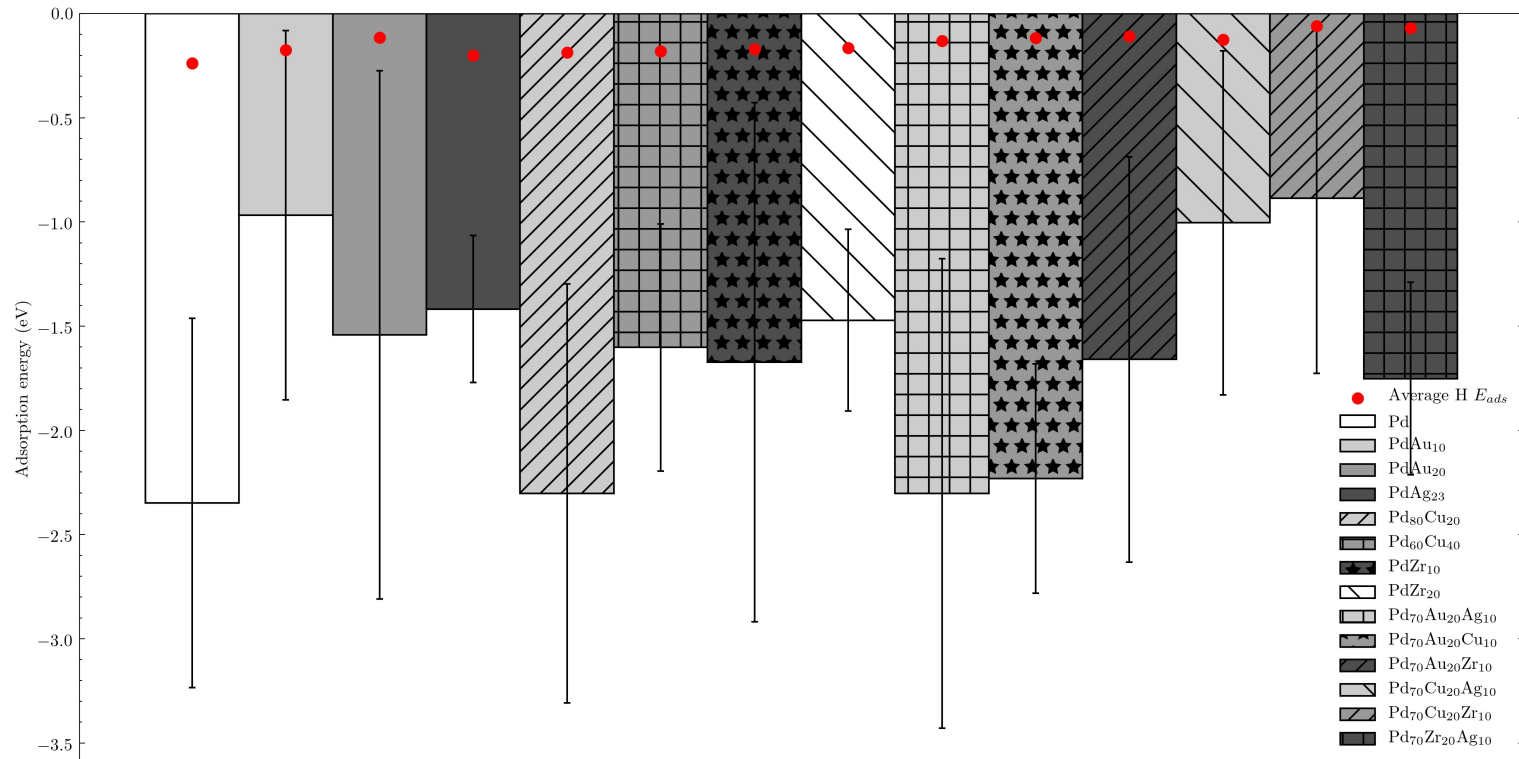


Figure 4.14: Average binding energy of formaldehyde on the surface of palladium and palladium alloy slabs

Formic Acid adsorption

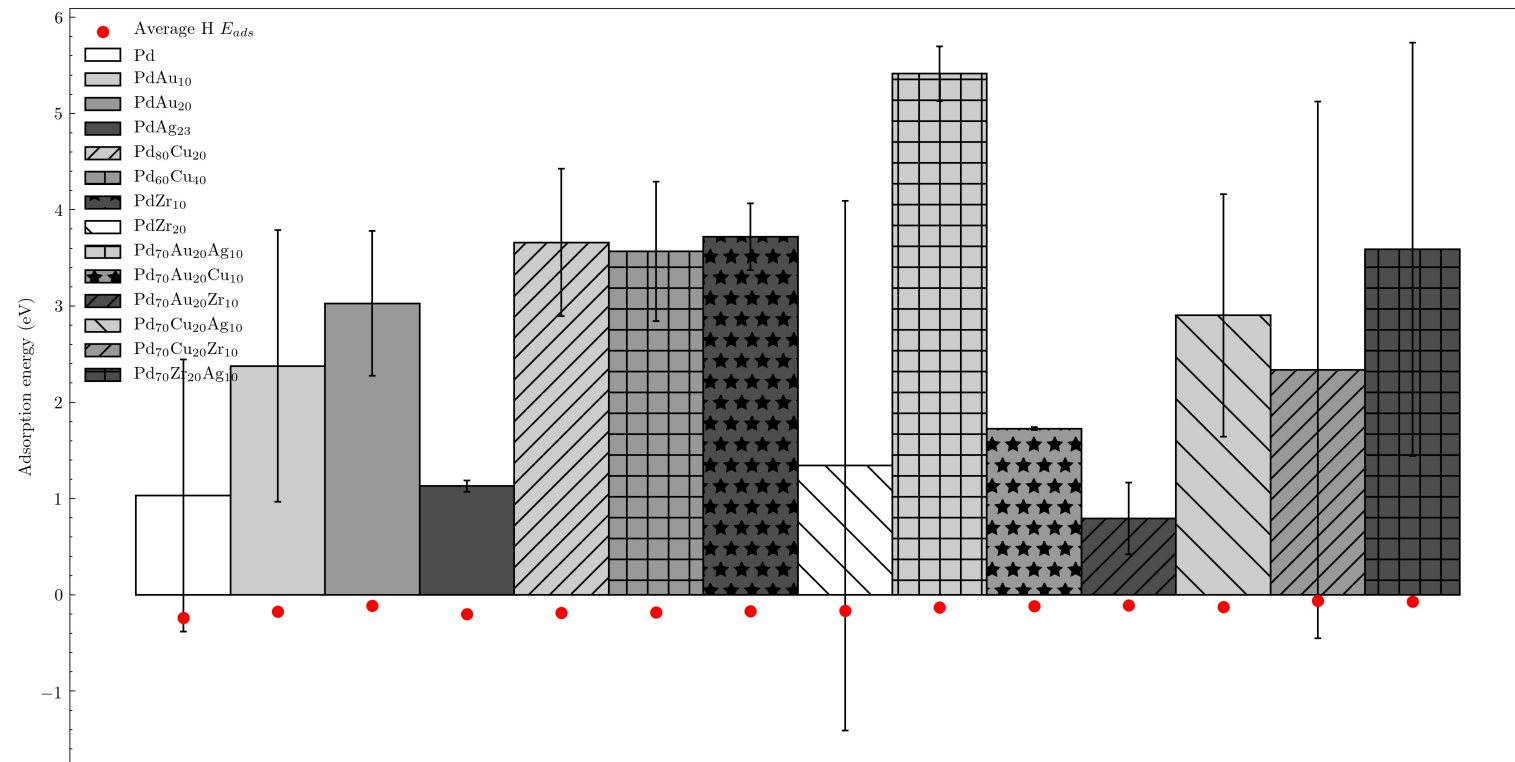


Figure 4.15: Average binding energy of Formic Acid on the surface of palladium and palladium alloy slabs

H₂S adsorption sites on Pd compared to H

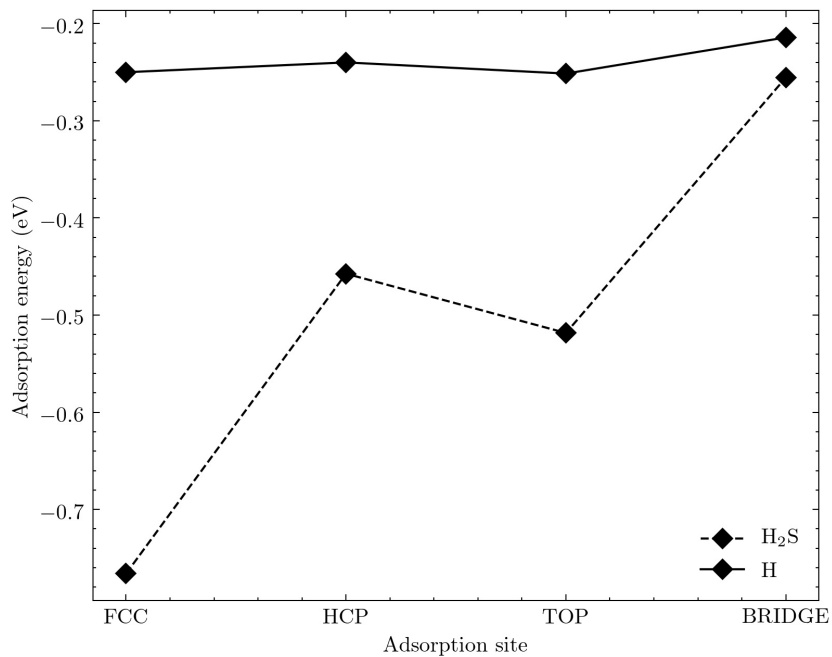


Figure 4.16: binding energy of H and H₂S for each site on a 2x2x5 Pd slab

Hydrogen sulphide

The final molecule that was simulated was H₂S. This molecule was adsorbed using the sulphur atom as this is the known mechanism for H₂S binding on a metallic surface. [29] The results are shown in figure 4.17. As expected all metals showed the ability to bind with the sulphur atom at least as strongly as hydrogen. Additionally the S atom will bind stronger to all active sites for hydrogen dissociation as shown by figure 4.16.

It appears that alloying with most metals will do little to halt the binding of sulphur, except for gold and Zr. Alloying with these metals brings the binding energy to a level where it is around equal to that of hydrogen, and is therefore more manageable. Additionally while alloying with silver on its own appears to infact increase the ability for sulphur to bind onto the surface, the effect is completely negated when gold is present.

Of the alloys tested PdAu₂₀, both Zr binary alloys, PdAuZr, PdCuAu, and PdZrCu appear to be the most suitable for mitigating the effects of H₂S. It should be noted that past studies have revealed that Pd₄S is in fact available for hydrogen permeation, albeit at a much slower rate.[29] This may indicate that it is possible to pretreat a palladium membrane with sulphur, to a point where it is no longer reactive to sulphur, but can still permeate hydrogen. Such studies are outside the scope of this thesis however

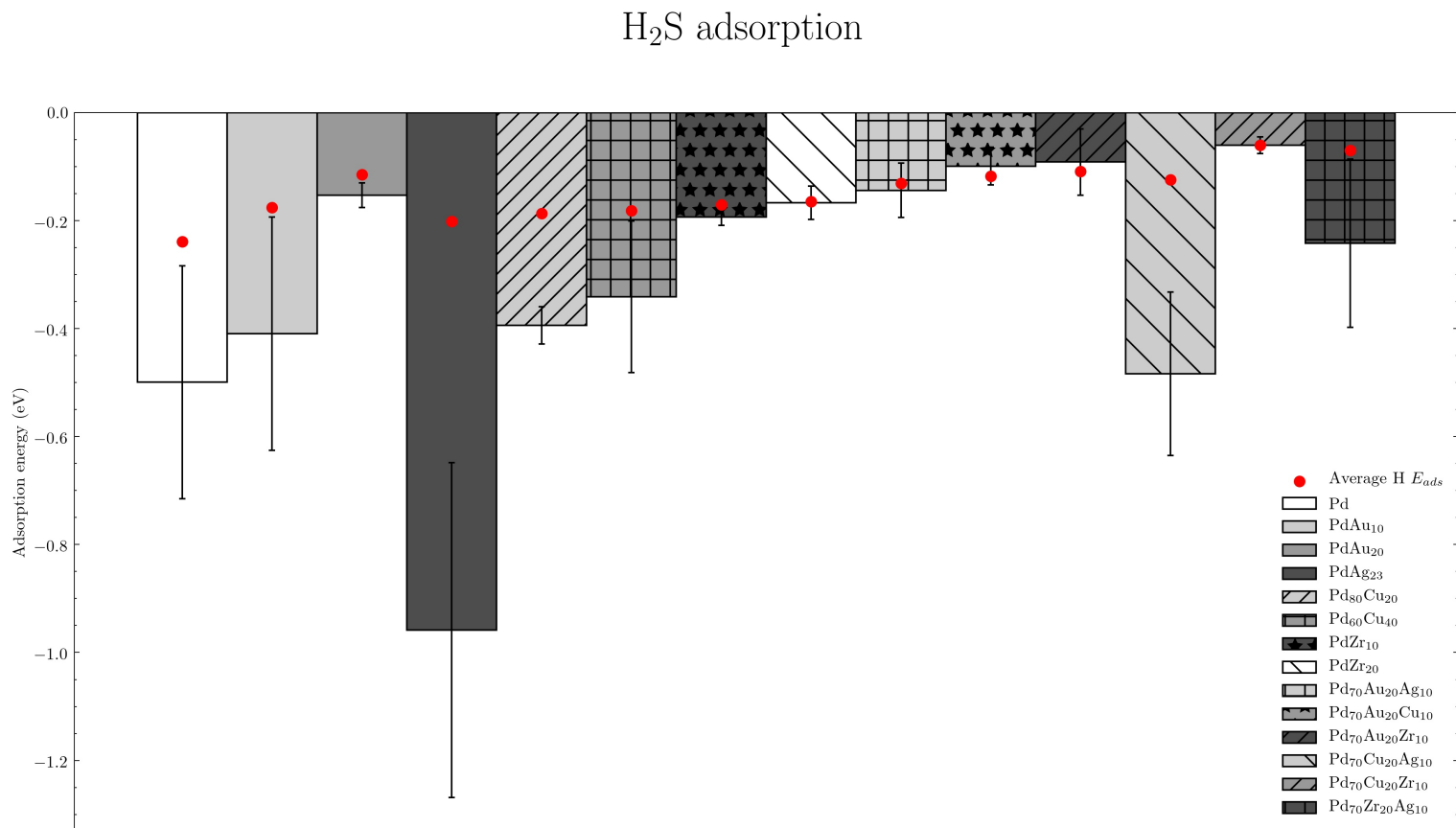


Figure 4.17: Average binding energy of H_2S on the surface of palladium and palladium alloy slabs

Table 4.4: Best performing alloys for each environment with respect to the different between the binding energies with relevant impurities, and the binding energy of hydrogen

Environment	Best performing alloy(s)	$E_{i_{ads}}/E_{H_{ads}}$ ($i=$ impurity)
Oxidising	PdAu20	-38.73 (H ₂ O), -7.18 (O ₂)
Carbonaceous	PdAu ₂₀	0.50(CO) 0.40 (CH ₄)
	PdAuCu	0.70(CO) 0.36(CH ₄)
	PdAuCu	0.84
Sulphurous	PdCuZr	0.92
	PdAuZr	0.98

4.4 Conclusion

DFT simulations were carried out investigating the binding energies of ISO 14687-2 impurities on the surface of palladium and palladium alloy membranes. A number of metals were alloyed, either because they are commonly used in literature, or are known for their resistance to sulphur containing environments which were of key importance to this thesis. Most alloys were found to be stable except for Cr containing alloys, which were eliminated from the study.

After testing the impurities it was clear that the binding of CO, CH₄, O₂, H₂O and H₂S were affected most by the alloy composition. Ar, He, N₂, NH₃, CO₂, and Formic acid were found to be completely inert to all compositions. Formaldehyde strongly adsorbed to all alloys regardless of composition and further research will have to be taken to find a suitable composition to mitigate this.

These impurities can be split into 3 broad groups, oxidising (O₂ and H₂O) carbonaceous (CH₄ and CO) and sulphurous (H₂). The best performing alloys for each of these impurities were decided by comparing the calculated binding energy to that of the same alloy binding with Hydrogen. The most suitable alloys for each class of material is shown in table 4.4.

In the following chapter these membraneanes will be manufactured and tested under carbonaceous and sulphur containing environments in order to validate the results of this study. Oxygen containing environments will not be tested due to the dangers of heating oxygen in a hydrogen matrix.

References

- [1] Paolo Giannozzi, Stefano Baroni, Nicola Bonini, Matteo Calandra, Roberto Car, Carlo Cavazzoni, Davide Ceresoli, Guido L Chiarotti, Matteo Cococcioni, Ismaila Dabo, Andrea Dal Corso, Stefano de Gironcoli, Stefano Fabris, Guido Fratesi, Ralph Gebauer, Uwe Gerstmann, Christos Gougaoussis, Anton Kokalj, Michele Lazzeri, Layla Martin-Samos, Nicola Marzari, Francesco Mauri, Riccardo Mazzarello, Stefano Paolini, Alfredo Pasquarello, Lorenzo Paulatto, Carlo Sbraccia, Sandro Scandolo, Gabriele Sclauzero, Ari P Seitsonen, Alexander Smogunov, Paolo Umari, and Renata M Wentzcovitch. Quantum espresso: a modular and open-source software project for quantum simulations of materials. *Journal of Physics: Condensed Matter*, 21(39):395502 (19pp), 2009. URL <http://www.quantum-espresso.org>.
- [2] P Giannozzi, O Andreussi, T Brumme, O Bunau, M Buongiorno Nardelli, M Calandra, R Car, C Cavazzoni, D Ceresoli, M Cococcioni, N Colonna, I Carnimeo, A Dal Corso, S de Gironcoli, P Delugas, R A DiStasio Jr, A Ferretti, A Floris, G Fratesi, G Fugallo, R Gebauer, U Gerstmann, F Giustino, T Gorni, J Jia, M Kawamura, H-Y Ko, A Kokalj, E Küçükbenli, M Lazzeri, M Marsili, N Marzari, F Mauri, N L Nguyen, H-V Nguyen, A Otero de-la Roza, L Paulatto, S Poncé, D Rocca, R Sabatini, B Santra, M Schlipf, A P Seitsonen, A Smogunov, I Timrov, T Thonhauser, P Umari, N Vast, X Wu, and S Baroni. Advanced capabilities for materials modelling with quantum espresso. *Journal of Physics: Condensed Matter*, 29(46):465901, 2017. URL <http://stacks.iop.org/0953-8984/29/i=46/a=465901>.
- [3] Paolo Giannozzi, Oscar Baseggio, Pietro Bonfà, Davide Brunato, Roberto Car, Ivan Carnimeo, Carlo Cavazzoni, Stefano de Gironcoli, Pietro Delugas, Fabrizio Ferrari Ruffino, Andrea Ferretti, Nicola Marzari, Iurii Timrov, Andrea Urru, and Stefano Baroni. Quantum espresso toward the exascale. *The Journal of Chemical Physics*, 152(15):154105, 2020. doi: 10.1063/5.0005082. URL <https://doi.org/10.1063/5.0005082>.
- [4] Haebin Shin, Minsung Baek, Youngsoo Ro, Changyeol Song, Kwan-Young Lee, and In Kyu Song. Improvement of sulfur resistance of pd/ce-zr-al-o catalysts for co oxidation. *Applied Surface Science*, 429:102 – 107, 2018. ISSN 0169-4332. doi: <https://doi.org/10.1016/j.apsusc.2017.05.198>. URL <http://www.sciencedirect.com/science/article/pii/S0169433217315519>. Materials Challenges in Alternative and Renewable Energy 2017(MCARE 2017).

- [5] P. Marcus and J.M. Grimal. The antagonistic roles of chromium and sulphur in the passivation of nicrfe alloys studied by xps and radiochemical techniques. *Corrosion Science*, 31:377 – 382, 1990. ISSN 0010-938X. doi: [https://doi.org/10.1016/0010-938X\(90\)90134-Q](https://doi.org/10.1016/0010-938X(90)90134-Q). URL <http://www.sciencedirect.com/science/article/pii/0010938X9090134Q>. Passivation of metals and semiconductors.
- [6] G. T. Kasun Kalhara Gunasooriya and Mark Saeys. Co adsorption on pt(111): From isolated molecules to ordered high-coverage structures. *ACS Catalysis*, 8(11): 10225–10233, 2018. doi: 10.1021/acscatal.8b02371. URL <https://doi.org/10.1021/acscatal.8b02371>.
- [7] Nong Xu, Sung Su Kim, Anwu Li, John R Grace, C Jim Lim, and Tony Boyd. Investigation of the influence of tar-containing syngas from biomass gasification on dense Pd and Pd–Ru membranes. *Powder Technology*, 290:132–140, 2016. doi: 10.1016/j.powtec.2015.08.037.
- [8] Lin Qin and Chao Jiang. First-principles based modeling of hydrogen permeation through Pd–Cu alloys. *International Journal of Hydrogen Energy*, 37(17):12760–12764, 2012. ISSN 03603199. doi: 10.1016/j.ijhydene.2012.06.029.
- [9] Ichiro Oda, Hirohito Ogasawara, and Masatoki Ito. Carbon monoxide adsorption on copper and silver electrodes during carbon dioxide electroreduction studied by infrared reflection absorption spectroscopy and surface-enhanced raman spectroscopy. *Langmuir*, 12(4):1094–1097, 1996. doi: 10.1021/la950167j. URL <https://doi.org/10.1021/la950167j>.
- [10] Sh.k. Shaikhutdinov, R. Meyer, M. Naschitzki, M. Baumer, and H.-J. Freund. Size and support effects for co adsorption on gold model catalysts. *Catalysis Letters*, 86 (4):211–219, Mar 2003. doi: 10.1023/a:1022616102162.
- [11] A. MAUREEN ROUHI. Organozirconium chemistry arrives. *Chemical & Engineering News Archive*, 82(16):36–39, 2004. doi: 10.1021/cen-v082n016.p036. URL <https://doi.org/10.1021/cen-v082n016.p036>.
- [12] Dennis B. Malpass. *Commercially Available Metal Alkyls and Their Use in Polyolefin Catalysts*, chapter 1, pages 1–28. 2010. ISBN 9780470504437. doi: 10.1002/9780470504437.ch1. URL <https://onlinelibrary.wiley.com/doi/abs/10.1002/9780470504437.ch1>.
- [13] Ying She, Sean C Emerson, Neal J Magdefrau, Susanne M Opalka, Catherine Thibaud-Erkey, and Thomas H Vanderspurt. Hydrogen permeability of sulfur tolerant Pd–Cu alloy membranes. *Journal of Membrane Science*, 452:203–211, 2014. doi: 10.1016/j.memsci.2013.09.025.
- [14] Sang Chul Yeo, Sang Soo Han, and Hyuck Mo Lee. Adsorption, dissociation, penetration, and diffusion of n₂ on and in bcc fe: first-principles calculations.

Phys. Chem. Chem. Phys., 15:5186–5192, 2013. doi: 10.1039/C3CP44367A. URL <http://dx.doi.org/10.1039/C3CP44367A>.

- [15] Sean-Thomas B Lundin, Taichiro Yamaguchi, Colin A Wolden, S Ted Oyama, and J Douglas Way. The role (or lack thereof) of nitrogen or ammonia adsorption-induced hydrogen flux inhibition on palladium membrane performance. *Journal of Membrane Science*, 514:65–72, 2016. doi: 10.1016/j.memsci.2016.04.048.
- [16] Jeffrey A. Herron, Scott Tonelli, and Manos Mavrikakis. Atomic and molecular adsorption on pd(111). *Surface Science*, 606(21):1670 – 1679, 2012. ISSN 0039-6028. doi: <https://doi.org/10.1016/j.susc.2012.07.003>. URL <http://www.sciencedirect.com/science/article/pii/S0039602812002245>.
- [17] Hui Li, Hengyong Xu, and Wenzhao Li. Study of n value and α/β palladium hydride phase transition within the ultra-thin palladium composite membrane. *Journal of Membrane Science*, 324(1-2):44–49, 2008. doi: 10.1016/j.memsci.2008.06.053.
- [18] Jerome Roques, Edouard Veilly, and Eric Simoni. Periodic density functional theory investigation of the uranyl ion sorption on three mineral surfaces: A comparative study. *International journal of molecular sciences*, 10:2633–61, 07 2009. doi: 10.3390/ijms10062633.
- [19] Sheng Meng, E. G. Wang, and Shiwu Gao. Water adsorption on metal surfaces: A general picture from density functional theory studies. *Phys. Rev. B*, 69:195404, May 2004. doi: 10.1103/PhysRevB.69.195404. URL <https://link.aps.org/doi/10.1103/PhysRevB.69.195404>.
- [20] Jia Chen and Annabella Selloni. Water adsorption and oxidation at the co₃O₄(110) surface. *The Journal of Physical Chemistry Letters*, 3(19):2808–2814, 2012. doi: 10.1021/jz300994e. URL <https://doi.org/10.1021/jz300994e>.
- [21] Thomas Bacquart, Niamh Moore, Nick Hart, Abigail Morris, Thor A. Aarhaug, Ole Kjos, Fabien Aupretre, Thibault Colas, Frederique Haloua, Bruno Gozlan, and Arul Murugan. Hydrogen quality sampling at the hydrogen refuelling station – lessons learnt on sampling at the production and at the nozzle. *International Journal of Hydrogen Energy*, 45(8):5565 – 5576, 2020. ISSN 0360-3199. doi: <https://doi.org/10.1016/j.ijhydene.2019.10.178>. URL <http://www.sciencedirect.com/science/article/pii/S0360319919340510>. 22nd World Hydrogen Energy Conference.
- [22] Hao Cui, Xiaoxing Zhang, Jun Zhang, and Muhammad Ali Mehmood. Interaction of co and ch₄ adsorption with noble metal (rh, pd, and pt)-decorated n₃-cnts: A first-principles study. *ACS Omega*, 3(12):16892–16898, 2018. doi: 10.1021/acsomega.8b02578. URL <https://doi.org/10.1021/acsomega.8b02578>.
- [23] Yuta Tsuji and Kazunari Yoshizawa. Adsorption and activation of methane on the (110) surface of rutile-type metal dioxides. *The Journal of Physical Chemistry C*,

122(27):15359–15381, 2018. doi: 10.1021/acs.jpcc.8b03184. URL <https://doi.org/10.1021/acs.jpcc.8b03184>.

- [24] International Standard ISO 14687-2: 2012. Hydrogen Fuel - Product Specification, 2012.
- [25] Arul Murugan and Andrew S Brown. Review of purity analysis methods for performing quality assurance of fuel cell hydrogen. *International Journal of Hydrogen Energy*, 40(11):4219–4233, 2015. doi: 10.1016/j.ijhydene.2015.01.041.
- [26] Dandan Wang, Yingying Fan, Zhonghui Sun, Dongxue Han, and Li Niu. A theoretical study of formaldehyde adsorption and decomposition on a wc (0001) surface. *RSC Adv.*, 8:32481–32489, 2018. doi: 10.1039/C8RA04983A. URL <http://dx.doi.org/10.1039/C8RA04983A>.
- [27] Longhui Nie, Jiaguo Yu, Mietek Jaroniec, and Franklin Feng Tao. Room-temperature catalytic oxidation of formaldehyde on catalysts. *Catal. Sci. Technol.*, 6:3649–3669, 2016. doi: 10.1039/C6CY00062B. URL <http://dx.doi.org/10.1039/C6CY00062B>.
- [28] Andrew Capon and Roger Parsons. The oxidation of formic acid on noble metal electrodes: Ii. a comparison of the behaviour of pure electrodes. *Journal of Electroanalytical Chemistry and Interfacial Electrochemistry*, 44(2):239 – 254, 1973. ISSN 0022-0728. doi: [https://doi.org/10.1016/S0022-0728\(73\)80250-5](https://doi.org/10.1016/S0022-0728(73)80250-5). URL <http://www.sciencedirect.com/science/article/pii/S0022072873802505>.
- [29] Bryan D Morreale, Bret H Howard, Osemwengie Iyoha, Robert M Enick, Chen Ling, and David S Sholl. Experimental and Computational Prediction of the Hydrogen Transport Properties of Pd 4 S. *Ind. Eng. Chem. Res.*, 46:6313–6319, 2007.

Chapter 5

Impurity resistance of dense metal membranes under hydrogen impurities

5.1 Abstract

In this chapter a number of dense palladium alloy membranes were synthesised on a YSZ substrate using a combination of electroless plating and magnetron sputtering in order to determine which membrane compositions resisted impurities.

The permeability of the synthesised membranes, in addition to a commercial membrane were tested under a variety of ISO 14687-2 impurities in order to determine which alloy composition was most suitable for use as a membrane material for hydrogen impurity enrichment, where low reactivity with impurities present in hydrogen samples are required. Of the tested membranes the best performing compositions were PdAuAg, PdAuCu and PdCuZr which only showed a 27%, 25% and 26% drop in permeability under atmospheres containing 10 ppm of non-sulphurous, and 2 ppm of sulphurous impurities typically expected to be found in hydrogen derived from steam methane reforming. This indicates that these alloys are most suitable for metrology purposes due to their low reactivity.

5.2 Introduction

In order to improve the accuracy and the cost of hydrogen impurity enrichment a suitable membrane composition must be found. In addition to this all previous studies used a commercial palladium-based membrane and in all cases it was noted that certain impurities reacted with the membrane. This interaction had the result of changing the composition of the enriched gas mixture and therefore reducing the final accuracy of the measurement. [1, 2] The self-supported commercial membranes used in both studies are also generally between 20-100 μm in order to provide sufficient mechanical strength for a membrane. However, for palladium membranes to be economical this thickness must

be reduced to about 1-5 μm giving the added benefit of greater flux and therefore lower enrichment times.

Palladium alloy membranes are generally created by forming an alloy with silver, copper or gold. By doing this the hydrogen embrittlement effect can be effectively mitigated. Using alloys has the added benefits of decreasing the overall amount of palladium required in the film, driving up their cost effectiveness, and in some cases increasing the flux of the membrane to higher levels achievable than a pure palladium membrane. In the previous chapter a number of membrane compositions were identified to be able to resist certain classes of ISO 14687-2 impurities. The best membranes being identified as PdAu_{20} and $\text{PdAu}_{20}\text{Cu}_{10}$ for carbonaceous impurities. For sulphur containing impurities $\text{PdCu}_{20}\text{Zr}_{10}$, $\text{PdAu}_{20}\text{Zr}_{10}$, and $\text{PdAu}_{20}\text{Cu}_{10}$ were the most resistant to binding with H_2S . In this chapter these membranes will be manufactured and tested under environments containing these gases in order to verify these results, and quantify the level of reactivity. In addition to these alloys, $\text{PdCu}_{20}\text{Ag}_{10}$ and $\text{PdAu}_{20}\text{Ag}_{10}$ will be synthesised due to their strong performance in the previous chapter. PdAg_{23} , PdCu_{20} and PdCu_{40} will also be synthesised as these are popular membrane compositions in literature and act as a good benchmark in addition to the commercial membrane. Unfortunately the PdAuZr composition could not be manufactured due to the high cost associated with sputtering gold.

Palladium alloy membranes will be deposited onto porous YSZ supports using both electroless plating and closed field unbalanced magnetron sputter ion plating as described in sections 3.2.3 and 3.2.3. This will have the combined effect of reducing the amount of palladium used, driving down their cost, and increasing the flux, and therefore reducing the time taken to enrich a hydrogen sample. The degree of interaction of impurities with the surface of the membrane will be quantified using a three-step experimental procedure. The pure hydrogen flux of each membrane composition will be measured and the membranes hydrogen permeability calculated as a base line. The following two permeation tests will measure the change in permeability resulting from introducing part-per-million level impurities into the gas sample. The change in permeability which results from this will act as a measure for the membranes tendency to interact with different impurity types. Additionally, at all three testing stages, X-ray photoelectron spectroscopy (XPS) will be performed on the surface of the membranes to investigate how the composition on the surface of the membrane changes when exposed to each impurity environment. This will allow the alloy segregation behaviour to be observed, and more importantly, quantify the amount of sulphur which has reacted with the surface of the membrane.

5.3 Results and Discussion

5.3.1 Membrane characterisation

Figure 5.1 (a)-(g) shows the cross-sectional SEM images of the manufactured membranes. The thickness of the fabricated membranes are shown in 5.1 and ranged from 573 nm

Table 5.1: Membrane compositions analysed by EDS and their thickness measured using FIB-SEM

Membrane ID	Manufacturing technique	Composition (wt%) (+- 1% Relative)					Thickness (um)
		Pd	Cu	Ag	Au	Zr	
PdCu (Fcc)	Magnetron Sputtering	76.24	23.76	-	-	-	1.679
PdCu (Bcc)	Magnetron Sputtering	43.24	56.64	-	-	-	1.664
PdCuZr	Magnetron Sputtering	72.10	14.46	-	-	13.54	1.541
PdAg	Electroless Plating	65.55	-	34.45	-	-	0.573
PdAu	Electroless Plating	74.7	-	-	25.3	-	1.172
PdCuAg	Electroless Plating	72.1	-	8.27	19.58	-	0.867
PdCuAu	Electroless Plating	63.90	13.6	-	22.1	-	1.545
PdAuAg	Electroless Plating	60	-	11.2	28.3	-	0.736

to $1.579 \mu\text{m}$. In general thinner layers were achieved using electroless plating although theoretically sub-micron layers are possible through magnetron sputtering, examples of this being SINTEF's patented sputtering process.[3] The integrity of the manufactured membranes was measured using the procedure laid out in section 3.2.4. All membranes showed no leakage when pressurised to 10 bar indicating that all membranes were uniform, pinhole free and therefore suitable for hydrogen separation. [4]

The surface composition of each membrane was measured by XPS and is shown in Table 5.1. A wide range of compositions were fabricated. From phase data on the PdCu system [5, 6] both varieties of PdCu membranes (bcc phase and fcc phase) were successfully fabricated.

5.3.2 Hydrogen permeation

Table 5.2 shows the hydrogen permeation through the 9 tested membranes at steady state after 12 hours of operation. As expected, hydrogen permeation flux increases with the elevated temperatures. Moreover, the mass transfer resistance of the substrate will not represent major limitations since its gas transport resistance is negligible compared to that of the dense palladium alloy layer [4]. Deposited layers were all on the scale of $0.5\text{-}2 \mu\text{m}$ which from previous research indicates the main rate limiting step in hydrogen permeation being the thickness of the membrane layer. [7] The palladium copper alloy which was in the bcc phase showed the highest hydrogen permeability of all the synthesised membranes which was expected as discussed in section 2.5.1. The membrane which showed the lowest hydrogen permeability was the PdCuZr membrane, this is likely due to the combined effects of the alloy having the lowest concentration of palladium compared to the other synthesised membrane, increasing the transport resistance of the membrane, and this composition having a lower preference to hydrogen binding as all other palladium alloys as predicted in the simulations performed in section 4.3.2 and shown in figure 4.2. The PdAu and PdAuAg membranes both showed low permeabilities. Gold as an alloying material traditionally does not show much increase in permeability [8] but is instead used to suppress the effects of impurities on the mem-

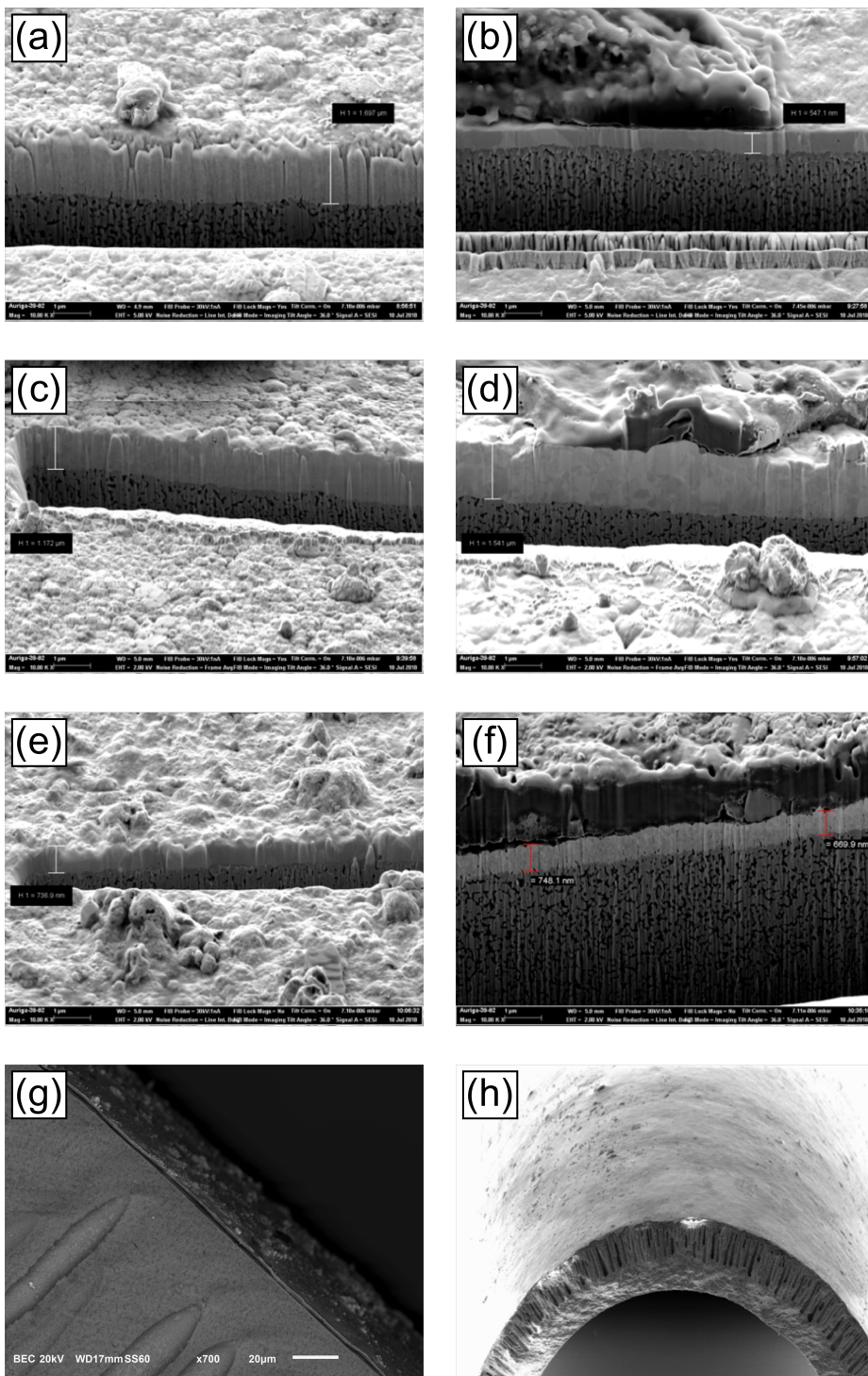


Figure 5.1: SEM images of fabricated membranes (a) PdCu (fcc) (Sputtering) (b) PdAg (ELP) (c) PdAu (ELP) (d) PdCuZr (Sputtering) (e) PdAgAu (ELP) (f) PdCuAg (ELP) (g) PdCu (bcc) (Sputtering) (h) typical cross section

Table 5.2: Pure hydrogen permeability of studied alloy membranes under pure hydrogen at 300°C and 1 bar pressure differential

Membrane ID	Permeability ($mol\ m^{-1}s^{-1}pa^{1/2} \times 10^{-8}$)
PdCu (Fcc)	1.30
PdCu (Bcc)	1.68
PdCuZr	0.14
PdAg	0.94
PdAu	0.33
PdCuAg	1.22
PdCuAu	1.43
PdAuAg	0.19
Commercial (REB)	5.71

Table 5.3: Permeability results for all membranes under both impurity conditions

Membrane ID	Permeability ($mol\ m^{-1}s^{-1}pa^{1/2} \times 10^{-8}$)			% Drop	
	Pure H ₂	Non-Sulphur	Sulphur	Non-sulphur	Sulphur
PdCu (Fcc)	1.30	0.22	0.185	80%	86%
PdCu (Bcc)	1.68	0.721	2.47	55%	85%
PdCuZr	0.14	0.12	0.101	12%	26%
PdAg	0.94	0.117	0.007	88%	92%
PdAu	0.33	0.165	0.215	51%	35%
PdCuAg	1.22	0.48	0.299	61%	75%
PdCuAu	1.43	0.789	1.07	45%	25%
PdAuAg	0.19	0.163	0.142	16%	27%

brane, [8] which is the main goal of this study. Despite the fact that the commercial membrane is also based on PdAgAu, the membrane manufactured through electroless plating has a lower permeability due to the high gold concentration. It is likely that the concentration of silver in the commercial membrane is closer to 23%, which is the optimal value for hydrogen permeation, and it's gold concentration is much lower than the electroless plated membrane. Both PdCuAg and PdCuAu had reasonably high hydrogen permeabilities. While none of these membranes showed a hydrogen permeability as high as the commercial alloy, it should be noted that the commercial membrane had a much larger thickness resulting in a much higher cost and lower flux values than the composite membranes.

5.3.3 Impurity reactivity

Table 5.3 shows the results of hydrogen permeation under the presence of the two different impurity conditions discussed in Table 5.3 compared to the pure hydrogen permeability values shown in Table 5.2. The permeability data was taken once the flux had reached steady state after 12 hours of operation. For all membranes there was a reduction in permeability when the membranes were exposed to impurities. The magnitude of this reduction compared to the pure hydrogen permeability is used as an indication of the degree of interaction between the membrane and the impurities. Table 5.4 shows the composition of each membrane in between each test in order to measure permanent surface reactions and segregation behaviour of the alloys under the chosen impurities.

Binary alloys

In non-sulphur tests the PdAg binary alloy was the worst performing, with the permeability dropping by 88% of its original value. This was expected as the addition of silver to a palladium system, while effective at increasing the permeability, does not contribute much to impurity resistance. [9] This was further supported by the results of the sulphur tests where the permeability dropped by 92% and composition analysis in Table 5.4 showing that sulphur was present in 42% of the surface. The PdAg alloy also showed a large degree of segregation behaviour under non-sulphur impurities which likely contributed to the large reduction in flux, with silver concentration increasing to 75% at the top 10 nm of the sample, resulting in a large drop in permeability.

Interestingly the PdCu membrane with a composition in the bcc phase showed higher resistance to non-sulphurous impurities than the fcc phase, with the former only experiencing a 55% drop in permeability compared to an 80% drop in permeability in the latter. This again seems to be a result of the segregation behaviour of the alloy, with the PdCu alloy in the fcc phase experiencing a large amount of segregation, with the palladium concentration increasing to around 90% on the retentate side. Conversely the PdCu composition in the BCC phase membrane only changed slightly. The XPS analysis showed that while the reactivity of sulphur on the surface of both copper based binary membranes was of a similar magnitude, the BCC phase had a slightly lower resistance, with 29% of the surface containing sulphur after exposure to sulphurous impurities as opposed to the 25% shown by the fcc phase alloy.

The PdAu alloy showed the best impurity resistance out of the binary alloys tested under both impurity conditions, with only a 51% and 35% drop in permeability under non-sulphur and sulphur conditions respectively and only a 12% concentration of sulphur was observed on the surface after XPS analysis. The alloy showed slight segregation of gold away from the permeate surface under non-sulphur impurity conditions likely due to the fact the difference in interaction strength between gold and palladium with the components of the gas mixture varies widely, with many gases preferentially adsorbing on palladium [10].

Table 5.4: XPS composition analysis of the palladium alloy membrane surfaces after impurity tests

Membrane ID	Pure Hydrogen Exposure					Non-Sulphur Exposure					Sulphur Exposure					
	Pd	Ag	Au	Cu	Zr	Pd	Ag	Au	Cu	Zr	Pd	Ag	Au	Cu	Zr	S
PdCu (Fcc)	65.5	-	-	35.5	-	92.5	-	-	7.5	-	67.5	-	-	7.5	-	25
PdCu (Bcc)	44	-	-	66	-	54.85	-	-	45.15	-	40	-	-	31	-	29
PdCuZr	63.6	-	-	22.6	13.8	64.4	-	-	27.5	8.5	54.2	-	-	27	8	10.8
PdAg	65.5	34.5	-	-	-	25	75	-	-	-	29	29	-	-	-	42
PdAu	75	-	25	-	-	82.9	-	17.1	-	-	71	-	16	-	-	13
PdCuAg	64.6	9.1	-	26.3	-	8.6	8.9	-	82.5	-	6	5	-	64	-	25
PdCuAu	63.9	-	22.5	13.6	-	84.9	-	1.46	13.6	-	65.3	-	1	18.5	-	15.2
PdAuAg	60	11.7	28.3	-	-	47.2	49.8	3	-	-	52	35	1	-	-	12

Ternary alloys

Five ternary alloy compositions were tested including the commercial alloy. The commercial alloy had the highest permeability of all ternary alloys with a value of $5.71 \text{ mol m}^{-1} \text{ s}^{-1} \text{ pa}^{-0.5} \times 10^{-8}$ under pure hydrogen and $4.28 \text{ mol m}^{-1} \text{ s}^{-1} \text{ pa}^{-0.5} \times 10^{-8}$ under non-sulphur conditions, a drop in permeability of 25%. However, the commercial membrane nearly lost all of its permeability under sulphurous conditions. The PdAuAg membrane manufactured through electroless plating performed better under both impurity conditions than the commercial alloy despite being based on the same composition, only seeing a 16% and 27% drop in hydrogen permeability under non-sulphur and sulphur conditions respectively compared to a 25% and 96% drop shown by the commercial alloy. The high levels of gold likely contributed to the low levels of sulphur on the surface of the electroless plated PdAuAg membrane. These results indicate that the composition of the commercial membrane, while ideal for separation, does not contain enough gold to withstand the levels of sulphur impurities expected for analytical purposes.

The worst performing ternary alloy was the PdCuAg alloy which showed large permeability drops under all conditions, 61% under non-sulphur and 75% under sulphurous conditions. In addition to these, large degrees of segregation were observed under non-sulphur impurities, with the palladium concentration at the surface dropping to 8.5 wt%, showing that the alloy is not completely stable under the varying conditions expected during analytical purposes.

Both gold containing ternary alloys, PdAuAg and PdCuAu, performed well under sulphur conditions, with the PdCuAu alloy only reducing in permeability by 25% and the PdAgAu membrane by 27%. The PdCuAu membrane however had a stronger interaction with non-sulphur impurities, indicated by the permeability drop of 45% when exposed to the non-sulphur containing gas sample. This drop is likely due to the segregation of palladium to the surface with the XPS data indicating an increase of palladium to the surface to 84.9 wt% from 63.9%. The best performing ternary membrane was the PdCuZr membrane which showed the smallest drop in permeability of only 12% non-sulphur conditions, and a permeability percentage drop of 26% under sulphur conditions which on a similar magnitude to that of the gold containing alloys.

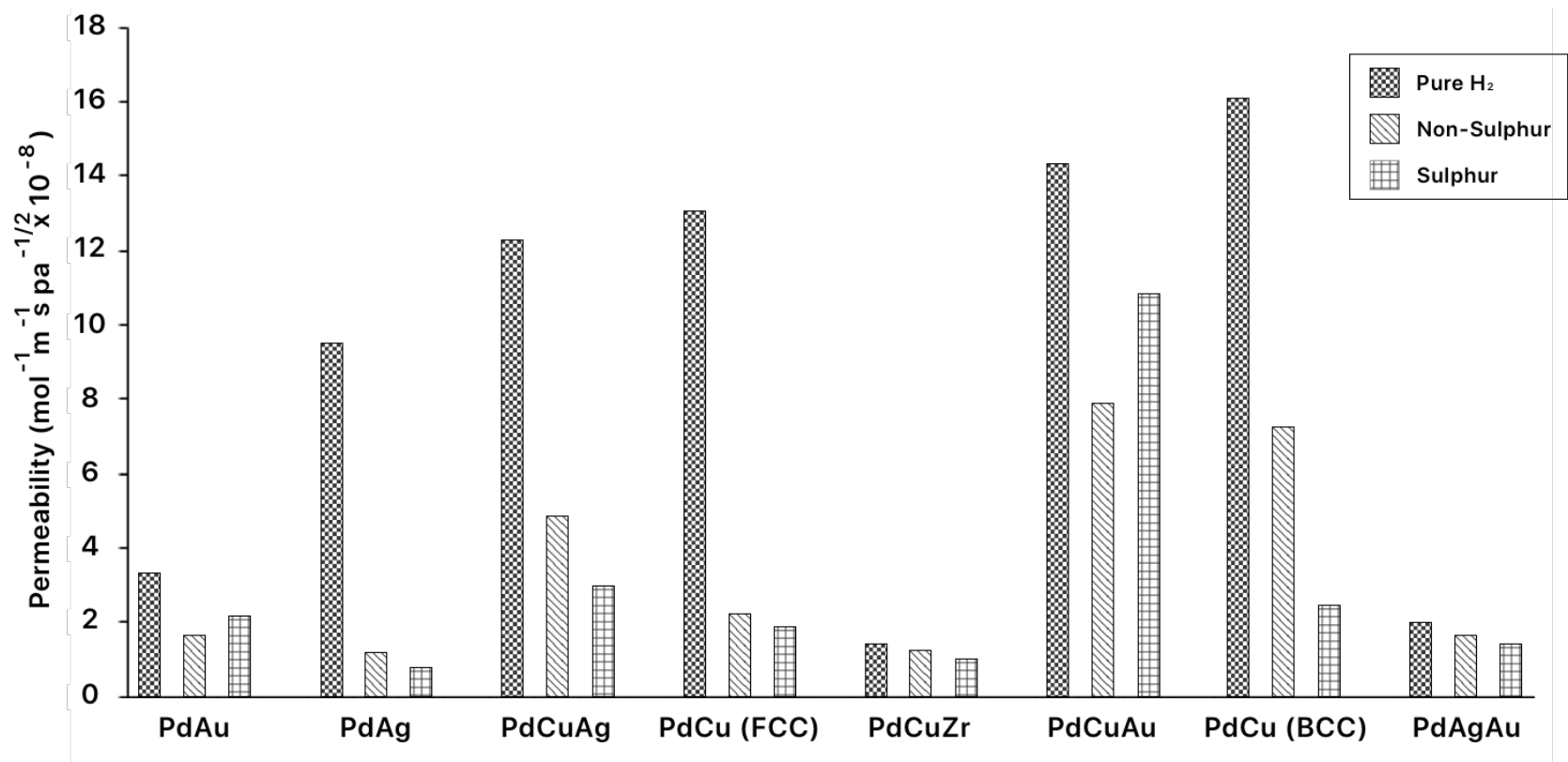


Figure 5.2: Permeability data for pure hydrogen, non-sulphur, and sulphur permeation tests

Segregation behaviour

All membranes tested showed some degree of segregation with the two thinnest membrane samples, PdAg (0.573 micron), PdAuAg (0.736 micron) and PdCuAg (0.873 micron) all showing the highest degrees of segregation. While this may still be a property of the alloy compositions it may also indicate that sub-micron palladium alloys layers are unstable and there may be a minimum thickness for alloys, below which the membrane layer is unstable and frequently varies during operation.

5.3.4 Relationship to DFT results

The previous chapter attempted to use DFT generated binding energies to predict the performance of alloy compositions in environments containing ISO 14687-2 impurities. While a useful analysis it appears in some cases that these results were not completely correct and could be improved in further studies.

For carbonaceous environments the model predicted that PdAu₂₀ and PdAuCu would be the best performing alloys. PdAuCu experienced a 45% drop in permeability under carbonaceous environments while PdAu₂₀ experienced a 51% drop. Which while showing reasonable resistance, were inferior to both the PdCuZr and PdAuAg alloys which only experienced a 12% and 16% drop respectively. For the PdAuAg alloy the model did indeed predict that it would resist adsorption to these impurities, and agrees with the conclusion of this analysis that the addition of gold and silver improves the alloys resistance to carbonaceous impurities. However appears to be completely incorrect, with all models predicting that the alloy would be more susceptible to poisoning.

The model fared better when predicting the influence of sulphurous impurities on the surface of the membrane. The model successfully predicted that both PdCuAu and PdCuZr alloys would be the most resistant to sulphurous environments. The model appears to be accurate in predicting how the other alloys would react in the environment, indicating the PdAg, PdCuAg, and both FCC and BCC PdCu alloys would perform poorly and see severe levels of sulphur poisoning. It should be noted that many of the results in this section were close and other alloys which performed reasonably well against sulphur poisoning (PdAu₂₀ and PdAuAg) could be as a result of the error between simulations.

The DFT simulations were a useful tool in predicting the sulphur resistance of the alloys, however when used to predict the behaviour of weaker adsorbing compounds, such as the carbonaceous impurities, it appears to break down. This is likely due to the fact that DFT is not as effective at simulating the behaviour of weaker bonds as discussed in section 2.6.2. Alternative methods should be explored if these interactions are to be predicted.

5.4 Conclusion

In order to identify a suitable palladium alloy composition for hydrogen impurity enrichment, eight different membrane compositions were manufactured and tested under three

different hydrogen conditions against a commercial palladium membrane. Two different measures were used to compare the membrane compositions suitability for hydrogen impurity enrichment, the permeability deviation from the pure hydrogen permeability was used as an initial indicator of interaction between the alloy and impurities, and the surface composition was measured to detect any impurities which had permanently reacted with the membrane.

The best performing membrane, and therefore the most suitable for hydrogen impurity enrichment was the PdCuZr alloy, which only showed a 12% and 26% drop in permeability under non-sulphur, and sulphur conditions, and low levels of sulphur on the surface. The permeability of this alloy was low, however, surface areas could easily be scaled up to increase the speed of hydrogen enrichment.

In the following chapter this membrane will be used in the design of the hydrogen impurity enrichment device and it's performance measured when tested with a real hydrogen fuel sample.

References

- [1] Arul Murugan and Andrew S Brown. Advancing the analysis of impurities in hydrogen by use of a novel tracer enrichment method. *Analytical Methods*, 6(15):5472, 2014. doi: 10.1039/c3ay42174k.
- [2] Shabbir Ahmed, Sheldon H D Lee, and Dionissios D Papadias. Analysis of trace impurities in hydrogen: Enrichment of impurities using a H₂ selective permeation membrane . *International Journal of Hydrogen Energy*, 35(22):12480–12490, 2010. doi: 10.1016/j.ijhydene.2010.08.042.
- [3] T. A. Peters, T. Kaleta, M. Stange, and R. Bredesen. Development of thin binary and ternary Pd-based alloy membranes for use in hydrogen production. *Journal of Membrane Science*, 383(1-2):124–134, 2011. ISSN 03767388. doi: 10.1016/j.memsci.2011.08.050. URL <http://dx.doi.org/10.1016/j.memsci.2011.08.050>.
- [4] Ana Gouveia Gil, Miria Hespanhol M Reis, David Chadwick, Zhentao Wu, and K Li. A highly permeable hollow fibre substrate for Pd/Al₂O₃ composite membranes in hydrogen permeation. *International Journal of Hydrogen Energy*, 40(8):3249–3258, 2015. ISSN 0360-3199. doi: <https://doi.org/10.1016/j.ijhydene.2015.01.021>. URL <http://www.sciencedirect.com/science/article/pii/S0360319915000580>.
- [5] Fernando Roa and J Douglas Way. Influence of Alloy Composition and Membrane Fabrication on the Pressure Dependence of the Hydrogen Flux of Palladium-Copper Membranes. *Ind. Eng. Chem. Res*, 42(23):5827–5835, 2003. ISSN 08885885. doi: 10.1021/ie030426x.
- [6] Shahrouz Nayebossadri, John Speight, and David Book. Development of Pd – Cu Membranes for Hydrogen Separation Why Hydrogen Separation ? 2013.
- [7] Tina M Nenoff Nathan W. Ockwig. Membranes for Hydrogen Separation. *Chemical Reviews*, 107:4078–4110, 2007.
- [8] Chao-Huang Chen and Yi Hua Ma. The effect of H₂S on the performance of Pd and Pd/Au composite membrane. *Journal of Membrane Science*, 362(1-2):535–544, 2010. doi: 10.1016/j.memsci.2010.07.002.
- [9] T A Peters, J M Polfus, M Stange, P Veenstra, A Nijmeijer, and R Bredesen. H₂ flux inhibition and stability of Pd-Ag membranes under exposure to trace amounts

of NH₃. *Fuel Processing Technology*, 152:259–265, 2016. doi: 10.1016/j.fuproc.2016.06.012.

- [10] Sabina K. Gade, Sarah J. DeVoss, Kent E. Coulter, Stephen N. Paglieri, Gökhan O. Alptekin, and J. Douglas Way. Palladium-gold membranes in mixed gas streams with hydrogen sulfide: Effect of alloy content and fabrication technique. *Journal of Membrane Science*, 378(1-2):35–41, 2011. ISSN 03767388. doi: 10.1016/j.memsci.2010.11.044. URL <http://dx.doi.org/10.1016/j.memsci.2010.11.044>.